

Chapter 4

X-ray Dichroisms in Spherical Tensor and Green's Function Formalism



Hebatalla Elnaggar, Pieter Glatzel, Marius Retegan, Christian Brouder, and Amélie Juhin

Abstract In this book chapter, our goal is to provide experimentalists and theoreticians with an accessible approach to the measurement or calculation of X-ray dichroisms in X-ray absorption spectroscopy (XAS). We start by presenting the key ideas of different calculation methods such as density functional theory (DFT) and ligand-field multiplet (LFM) theory and discuss the pros and cons for each approach. The second part of the chapter is dedicated to the expansion of the XAS cross section using spherical tensors for electric dipole and quadrupole transitions. This expansion enables to identify a set of linearly independent spectra that represent the smallest number of measurements (or calculations) to be performed on a sample, in order to extract all spectroscopic information. Examples of the different dichroic effects which can be expected depending on the type of transitions and on the symmetry of the system are then given.

4.1 Introduction

4.1.1 The X-ray Absorption Cross Section

The X-ray absorption cross section is obtained by dividing the transition rate by the flux of photons and summing over all possible final states. It is given in (4.1) where $\hbar\omega$ is the photon energy, and α the fine structure constant. $I(E_I)$ and $F(E_F)$ are the initial and final state wave functions (energies), and T is the transition operator,

H. Elnaggar

Debye Institute for Nanomaterials Science, Utrecht University, 3584 CA Utrecht, The Netherlands

P. Glatzel · M. Retegan

European Synchrotron Radiation Facility, 71 Rue des Martyrs, 38000 Grenoble, France

Ch. Brouder · A. Juhin (✉)

Institut de Minéralogie, Physique des Matériaux et Cosmochimie, CNRS-Sorbonne Université, 4 Place Jussieu, 75252 Paris Cedex 05, France

e-mail: amelie.juhin@sorbonne-universite.fr

© The Author(s) 2021

H. Bulou et al. (eds.), *Magnetism and Accelerator-Based Light Sources*,

Springer Proceedings in Physics 262,

https://doi.org/10.1007/978-3-030-64623-3_4

$$\sigma_\omega = 4\pi^2\alpha\hbar\omega \sum_F \langle I|T^\dagger|F\rangle \langle F|T|I\rangle \delta(E_I + \hbar\omega - E_F). \quad (4.1)$$

The transition operator describes the interaction of photons with the system. In the case of an electromagnetic plane wave, the transition operator writes $T \propto e^{i\mathbf{k}\cdot\mathbf{r}} \left[\hbar\boldsymbol{\epsilon} \cdot \nabla - \frac{g}{2s}\mathbf{k} \times \boldsymbol{\epsilon} \right]$ where $\boldsymbol{\epsilon}$ is the polarization vector of the incident photon, and \mathbf{k} is the incident wave vector, g the gyromagnetic ratio ($g \approx 2$ for the electron), and s the electron spin [1]. The exponential in the transition operator can be expanded as a Taylor series

$$e^{i\mathbf{k}\cdot\mathbf{r}} \approx 1 + i\mathbf{k} \cdot \mathbf{r} - \frac{(\mathbf{k} \cdot \mathbf{r})^2}{2!} + \dots \quad (4.2)$$

The first term in the expansion approximates the interaction of the light with the atom as an electric dipole ($\langle F|T|I\rangle = \hbar\langle F|\boldsymbol{\epsilon} \cdot \nabla|I\rangle = -\frac{m(E_F - E_I)}{\hbar}\langle F|\boldsymbol{\epsilon} \cdot \mathbf{r}|I\rangle$). The second term gives rise to the electric quadrupole interaction ($-i\frac{m(E_F - E_I)}{\hbar}\langle F|\boldsymbol{\epsilon} \cdot \mathbf{r}\mathbf{k} \cdot \mathbf{r}|I\rangle$) and to the (negligible) magnetic dipole one ($-\frac{1}{2}\langle F|(\boldsymbol{\epsilon} \times \mathbf{k}) \cdot (\mathbf{L} + g\mathbf{s})|I\rangle$) [1], the third term is the octupole transition ($\frac{m(E_F - E_I)}{6\hbar}\langle F|(\boldsymbol{\epsilon} \cdot \mathbf{r})(\mathbf{k} \cdot \mathbf{r})^2|I\rangle$) [2], and so on. In this chapter, we focus on electric dipole and quadrupole transitions.

The summation over final states in (4.1) implies that one has first to calculate the ground state, all possible final states, and then compute the transition matrix elements between the ground state and the final states. This is not always the most efficient way to numerically calculate XAS. Instead, Green's function can be used to replace the summation over final states by a propagator of the transition operator. Hence $\sum_F |F\rangle \langle F| \delta(E_I + \hbar\omega - E_F) \rightarrow \frac{-1}{2\pi i}(G^+ - G^-)$ with $G^\pm(E_I + \hbar\omega) = \frac{1}{\hbar\omega - H_F + E_I \pm \frac{1}{2}i\Gamma}$, where H_F is the final state Hamiltonian. The ‘‘Fermi Golden Rule’’ can be expressed as in (4.3). Most modern codes calculating core level spectra use this expression

$$\sigma_\omega = -4\pi\alpha\hbar\omega \text{Im} \left[\langle I|T^\dagger G^+(E_I + \hbar\omega)T|I\rangle \right]. \quad (4.3)$$

Let us now discuss electric dipole transitions according to the first term of the expansion in (4.2). For electric dipole transitions we have $T = \boldsymbol{\epsilon} \cdot \mathbf{r}$. One can see from the expression of the transition operator that the cross section will depend on the orientation of the polarization vector ($\boldsymbol{\epsilon}$) with respect to the absorbing system (\mathbf{r}). The X-ray absorption spectrum measured on any sample is in fact the sum of several linearly independent spectra as will be discussed further in this chapter. They can be disentangled by macroscopically orienting the sample, e.g., by using a single crystal or orienting the magnetic moments. Consequently, one may wonder:

- How many independent spectra exist for a given system?
- What information do they give us about the absorbing system?

4.1.2 Definition of Dichroisms

X-ray dichroism can be defined as the difference in the X-ray absorption cross section measured for two orthogonal polarization states of the incident light. There exist different types of dichroism. Dichroism measurements can be classified according to the type of polarization used for the measurements into linear and circular. **Linear dichroism** (LD) is the difference measured with linearly polarized light, where in most cases the polarization vector is set parallel and perpendicular to an orientation axis, while **circular dichroism** (CD) is the difference measured with circularly polarized light (left handed and right handed).

Not all systems exhibit dichroism effects when the polarization of the light is changed. Certain symmetry conditions regarding the interaction operator between light and matter have to be satisfied for dichroism effects to occur, which brings us to the second classification of dichroism types. Two symmetry operations are essential for this classification:

- Time-reversal symmetry,
- Space inversion (also called parity).

Natural dichroism (ND) refers to dichroism effects that occur in non-magnetic systems where time-reversal symmetry is conserved (i.e., the system is even under time-reversal operation). Using linearly polarized light, one can measure **X-ray natural linear dichroism** (XNLD). On the other hand, using circularly polarized light, one can measure **X-ray natural circular dichroism** (XNCD) only for systems that do not have a centre of inversion (i.e., the system is of odd parity).

Magnetic dichroism (MD) relates to dichroism effects measured in magnetic (ferro, ferri, or antiferromagnetic) systems where time-reversal symmetry is broken either by spontaneous magnetic ordering in the sample or by the application of an external magnetic field. **X-ray magnetic linear dichroism** (XMLD) is parity-even and time-reversal even and **non-reciprocal linear dichroism** (NRLD) is parity-odd and time-reversal odd. Using circularly polarized light, **X-ray magnetic circular dichroism** (XMCD) and **X-ray magneto-optical dichroism** (XM χ D) effects can be measured. The former is parity-even and time-reversal odd while the later is parity-odd and time-reversal odd.

In magnetic materials, which will be discussed in this chapter, several cases are possible:

- In the case of centrosymmetric crystals with ferro- or ferrimagnetic properties, one can measure XMCD.
- In the case of centrosymmetric crystals with antiferromagnetic properties, XMLD can be measured.
- In the case of magnetized, non-centrosymmetric crystals, XM χ D and NRLD can be measured.

XMCD and XMLD measurements give, respectively, access to the average value of $\langle M \rangle$ and $\langle M^2 \rangle$ of the local magnetization for the absorber. On the other hand,

$\text{XM}\chi\text{D}$ and NRLD signals are related to moments that are more complex, the anapole orbital moment and other higher order moments.

4.1.3 The Many-Body Problem in Spectra Calculations

The calculation of an absorption spectrum is a formidable task: it requires the calculation of the ground state of the system, the excited states of the system, and the interaction of the system with the electromagnetic field (X-ray beam). This means that the theoretical approach required to calculate XAS has to be suitable for calculating the electronic structure in addition to properly considering the interaction with the electromagnetic field. Approximations have often to be made to calculate the absorption (or the scattering Kramers–Heisenberg) cross section and the spectroscopist therefore has to choose which theoretical approach is the most suitable for the problem at hand.

In principle, the ground and excited states can be determined by solving the Dirac equation which accounts for all relativistic effects and includes all possible interactions in the Hamiltonian. This full treatment provides a relativistic, many-body, extended description of the electronic states. Unfortunately, in practice, it is not possible to perform such a calculation as it is computationally very consuming. In most cases one solves instead the Schrödinger equation and introduces relativistic effects as perturbations (e.g., the spin-orbit interaction). Furthermore, one can make use of the Born–Oppenheimer approximation to separate the electronic properties of the system from the dynamics of the nuclei. In order to describe the electronic part of the wave function, various theoretical approaches can be used such as (i) the single-particle extended picture (DFT-based approaches), (ii) the many-body atomic picture (multiplet theory), and (iii) the many-body extended picture (beyond DFT methods).

4.1.3.1 The Single-Particle Extended Picture of Electronic States

DFT-based methods can be used to describe the electronic states using a single-particle extended picture. Although DFT methods should formally only apply to ground state calculations, they are often used for the calculation of excited states probed in core level spectroscopies. DFT methods simplify the ground state wave function of N electrons by replacing them with a fictitious, non-interacting system of independent electrons, that have the same electronic density as the real system. The correct charge density minimizes the total energy of the system. The Schrödinger equation is transformed into a system of equations (called the “Kohn–Sham equations”) with an effective Hamiltonian and wave functions, which are functions of only one space variable. This implies that DFT is essentially a single-particle approach, although some many-particle (many-body) interactions are contained in the exchange and correlation term of the electronic effective potential. The exact

analytical expression of this term is not known. This means that DFT can only be applied in an approximate form for example using the local density approximation (LDA) or the generalized gradient approximation (GGA)].

One can determine the ground state wave function by solving the Kohn–Sham equations which are constructed from the single-particle wave functions. The ground state wave function is therefore formed by a single Slater determinant. This is an important point because it limits the ability to treat a many-body response of the system described through a linear combination of Slater determinants. To illustrate this let us take an example with two electrons. Coupling $s = 1/2$ to $s = 1/2$ yields $S = 1$ or 0 . This corresponds to four $|S, Ms\rangle$ wave functions: $|S = 1, Ms = 1\rangle$, $|S = 1, Ms = -1\rangle$, $|S = 1, Ms = 0\rangle$, and $|S = 0, Ms = 0\rangle$. These functions need to meet the property of being anti-symmetric under particle exchange and it can be shown that only $|S = 1, Ms = 1\rangle$, $|S = 1, Ms = -1\rangle$ can each be expressed as a single Slater determinant. However, the $|S = 1, Ms = 0\rangle$ and $|S = 0, Ms = 0\rangle$ states can only be expressed as the combination of two Slater determinants and thus cannot be calculated in DFT.

One can group the various DFT-based methods according to their characteristics:

- Cluster or periodic: The Kohn–Sham equations can be solved either for a cluster centred around the absorbing atom (direct or real space methods) or starting from a unit cell of the crystal (or a multiple unit cell, which is called supercell) in order to take advantage of the 3D periodicity (reciprocal space methods).
- Self-consistency or not: The Kohn–Sham equations can be solved without or (preferably) with self-consistency, i.e., using an iterative cycle where two successive steps are mixed until a convergence criterion is reached to determine the charge density.
- Type of basis functions used to expand the orbital solutions of the Kohn–Sham equations: either localized functions [linear combination of atomic orbitals (LCAO), linear muffin-tin orbitals (LMTO)], or delocalized functions [plane waves (PW), full-potential linearized augmented plane waves (FLAPW)].
- Approximation made on the shape of the electronic potential: For example in LMTO or multiple scattering theory, the potential is approximated to be spherically symmetric in the atoms, and constant between them (muffin-tin). In full-potential methods [FLAPW, or projector augmented wave (PAW)-pseudopotentials], no approximation is made, which is generally preferable, even though it makes the calculations more consuming.

4.1.3.2 The Many-Body Atomic Picture of Electronic States

A Simple Introduction to the Many-Body Atomic Picture

Let us consider as an example a Cr^{3+} ion in an octahedral (O_h) environment. Here the solid is reduced to an atom embedded in a mean field known as the crystal field (CF) that mimics the effect of the inter-atomic interactions. The atomic electronic configuration is $1s^2 2s^2 2p^6 3s^2 3p^6 3d^3$. The degeneracy of the Cr 3d levels is lifted

due to the CF and the $3d$ orbitals are split into two groups: the e_g orbitals pointing towards the ligands and the t_{2g} orbitals pointing between the ligands. The number of possible electronic states is given by the number of allowed arrangements of three electrons into ten spin orbitals, i.e., $C_{10}^3 = 120$ microstates. The energy separation between these states arises due to the combined effect of: (i) CF splitting, (ii) electronic repulsions, and (iii) spin-orbit coupling, i.e., the multiplet effects. Electrons occupying closed shells do not actually contribute to the energy splitting of the electronic levels; there is only one way to completely fill a shell giving a single average energy of the configuration.

All these multiplet states can be further grouped in so-called *term symbols* (or spectroscopic terms) according to their energy, spin and orbital moments. The relative energy positions of these spectroscopic terms for a $3d^n$ transition metal ion in O_h CF (and neglecting $3d$ spin-orbit coupling) were calculated by Tanabe and Sugano and are available in several references (e.g., [3, 4]). Similar diagrams are available in [5] for symmetries lower than O_h , such as trigonal or tetragonal. The relative energies of the electronic states depend on the CF parameters as well as the Racah parameters that relate to the electronic repulsions. The determination of the spectroscopic terms becomes very complex when the spin-orbit coupling and Zeeman terms are included in the Hamiltonian and/or if lower symmetries are considered. LFM theory takes these effects into account and has been realized in several computer codes.

Key Ideas of Ligand-Field Multiplet Theory

Atomic multiplet theory, crystal field multiplet theory, and LFM theory (sometimes collectively referred to as the *multiplet theory*) are based on concepts that were developed in atomic physics and make use of group theory. One has to solve the Schrödinger equation for the ion with its N electrons in a given configuration

$$\hat{H}|g\rangle = E|g\rangle, \quad (4.4)$$

where \hat{H} is the Hamiltonian of the system for the chosen configuration, E and $|g\rangle$ are the eigenvalue and eigenstate, respectively. The different eigenstates are functions of N electrons, hence they are called many-body (or multi-electronic) states. The Hamiltonian is expressed as

$$\hat{H} = \hat{T} + \hat{V} + \hat{V}_{ee} + \hat{H}_{SO} + \hat{H}_{CF}, \quad (4.5)$$

where \hat{T} is the kinetic energy of the electrons, \hat{V} the Coulomb attraction between electrons and the nucleus, \hat{V}_{ee} the electron–electron Coulomb interaction, \hat{H}_{SO} the spin-orbit coupling interaction, and \hat{H}_{CF} the CF Hamiltonian, which takes into account the local environment of the absorbing atom.

These interactions will now be expressed in second quantization formalism. In this notation, any operator can be expressed in terms of creation (c_τ^\dagger) and annihilation (c_τ) operators. The operator c_τ^\dagger creates a state characterized by the quantum numbers τ (for example, if we choose to express the states as spin-orbitals, τ will be the set

of quantum numbers n, l, m, σ that give the principal quantum number, the orbital momentum, the projected orbital momentum, and the projected spin momentum that uniquely identify this state) when it acts on the vacuum state $|0\rangle$. The operator c_τ is the annihilation operator of the state τ . In this formalism, the (spherical) atomic interactions write

$$\hat{T} = \sum_{\tau_1, \tau_2} \langle \tau_1 | \frac{\hat{p}^2}{2m} | \tau_2 \rangle c_{\tau_1}^\dagger c_{\tau_2}, \quad (4.6)$$

$$\hat{V} = \sum_{\tau_1, \tau_2} \langle \tau_1 | -\frac{Ze^2}{\hat{r}} | \tau_2 \rangle c_{\tau_1}^\dagger c_{\tau_2}, \quad (4.7)$$

$$\hat{V}_{ee} = \frac{1}{2} \sum_{\tau_1, \tau_2, \tau_3, \tau_4} \langle \tau_1 \tau_2 | \frac{e^2}{|\hat{r} - \hat{r}'|} | \tau_3 \tau_4 \rangle c_{\tau_2}^\dagger c_{\tau_1}^\dagger c_{\tau_3} c_{\tau_4}, \quad (4.8)$$

$$\hat{V}_{SO} = \sum_{\tau_1, \tau_2} \langle \tau_1 | \xi \hat{l} \cdot \hat{s} | \tau_2 \rangle c_{\tau_1}^\dagger c_{\tau_2}. \quad (4.9)$$

Here \hat{p} is the linear momentum operator, m is the electron mass, e is the electron charge, \hat{r} is the position operator, \hat{l} and \hat{s} are the orbital and spin momenta operators, and ξ is an atom dependent constant that is a function of the gradient of the atomic potential ($\xi \propto \frac{1}{r} \frac{dV}{dr}$). The kinetic energy of the electrons and the Coulomb interaction of the electrons with the nucleus are fixed for a given atomic configuration and they contribute only to the average energy of the configuration; hence \hat{T} and \hat{V} do not contribute to the multiplet splitting, and will not be further discussed. As a matter of fact, they are typically not evaluated in standard multiplet calculation programs. However, we are left with the task of simplifying the terms \hat{V}_{SO} and \hat{V}_{ee} . Let us start with \hat{V}_{SO} and assume that z is the quantization axis.

Influence of Spin-Orbit Coupling Interaction

The spin-orbit interaction is given as follows:

$$\begin{aligned} \hat{V}_{SO} &= \sum_{\tau_1, \tau_2} \langle \tau_1 | \xi (l_x s_x + l_y s_y + l_z s_z) | \tau_2 \rangle c_{\tau_1}^\dagger c_{\tau_2} \\ &= \sum_{\tau_1, \tau_2} \langle \tau_1 | \xi l_z s_z | \tau_2 \rangle c_{\tau_1}^\dagger c_{\tau_2} \\ &\quad + \sum_{\tau_1, \tau_2} \langle \tau_1 | \xi (l_x s_x + l_y s_y) | \tau_2 \rangle c_{\tau_1}^\dagger c_{\tau_2}. \end{aligned} \quad (4.10)$$

We shall use a set of atomic spin-orbitals as basis functions, $\psi_i = R_{n_i, l_i}(r) Y_{l_i, m_i}(\theta, \phi) \sigma_i$ where $Y_{l_i, m_i}(\theta, \phi)$ is the spherical harmonic, and $R_{n_i, l_i}(r)$ is the radial part. Given that the potential in ξ has a spherical form one can separate the radial and angular parts of the Hamiltonian. The angular part of the first term gives

$$\begin{aligned}
& \sum_{(l_1, m_1), (l_2, m_2)} \langle Y_{l_1, m_1} \sigma_1 | l_z s_z | Y_{l_2, m_2} \sigma_2 \rangle c_{l_1, m_1, \sigma_1}^\dagger c_{l_2, m_2, \sigma_2} \\
&= \frac{1}{2} \sum_{m=-l}^l m (c_{l, m, \uparrow}^\dagger c_{l, m, \uparrow} - c_{l, m, \downarrow}^\dagger c_{l, m, \downarrow}) . \tag{4.11}
\end{aligned}$$

The second term gives

$$\begin{aligned}
& \sum_{(l_1, m_1), (l_2, m_2)} \langle Y_{l_1, m_1} \sigma_1 | (l_x s_x + l_y s_y) | Y_{l_2, m_2} \sigma_2 \rangle c_{l_1, m_1, \sigma_1}^\dagger c_{l_2, m_2, \sigma_2} \\
&= \sum_{(l_1, m_1), (l_2, m_2)} \langle Y_{l_1, m_1} \sigma_1 | \frac{1}{2} (l^+ s^- + l^- s^+) | Y_{l_2, m_2} \sigma_2 \rangle c_{l_1, m_1, \sigma_1}^\dagger c_{l_2, m_2, \sigma_2} \tag{4.12} \\
&= \frac{1}{2} \sum_{m=-l}^{l-1} \sqrt{(l-m)(l+m+1)} (c_{l, m+1, \downarrow}^\dagger c_{l, m, \uparrow} + c_{l, m, \uparrow}^\dagger c_{l, m+1, \downarrow}) .
\end{aligned}$$

Hence the angular part of the spin-orbit Hamiltonian finally writes

$$\begin{aligned}
\hat{H}_{SO} &= \frac{1}{2} \sum_{m=-l}^l m (c_{l, m, \uparrow}^\dagger c_{l, m, \uparrow} - c_{l, m, \downarrow}^\dagger c_{l, m, \downarrow}) \\
&\quad + \frac{1}{2} \sum_{m=-l}^{l-1} \sqrt{(l-m)(l+m+1)} (c_{l, m+1, \downarrow}^\dagger c_{l, m, \uparrow} + c_{l, m, \uparrow}^\dagger c_{l, m+1, \downarrow}) . \tag{4.13}
\end{aligned}$$

It is clear from (4.13) that the spin-orbit interaction mixes states with different projected orbital and spin momenta.

The Electron–Electron Coulomb Interaction

Now we undertake the simplification of the electron–electron Coulomb interaction. This is more involved than the simplification of the spin-orbit coupling Hamiltonian. Cowan nicely explains the details of the derivation in his book [6]. We will rely on a combination of the derivations by Cowan [6] and Haverkort [7] in this section. This is not a thorough derivation; it is only meant to qualitatively explain the origin of multiplet splittings.

The first step to simplify this Hamiltonian is to perform a multipole expansion of the term $\frac{1}{\hat{r}-\hat{r}'}$ = $\sum_{k=0}^{\infty} \sum_{m=-k}^k Y_{k, m}^*(\theta', \phi') \frac{4\pi}{2k+1} \frac{r_{<}^k}{r_{>}^{k+1}} Y_{k, m}(\theta, \phi)$, where $r_{<}^k$ and $r_{>}^k$ are, respectively, the lesser and greater of the distances r and r' . Now we are in a position to separate the radial and angular terms of the expression and separate the angular variables of each electron. Using the atomic spin-orbital basis to express the matrix elements of the angular part of the Hamiltonian one finds that

$$\begin{aligned}
& \sum_{\tau_1, \tau_2, \tau_3, \tau_4} \langle Y_{l_1, m_1}(\theta, \phi) \sigma_1 Y_{l_2, m_2}(\theta', \phi') \sigma_2 | \sum_{k=0}^{\infty} \sum_{m=-k}^k Y_{k, m}^*(\theta', \phi') Y_{k, m}(\theta, \phi) | \\
& \qquad \qquad \qquad Y_{l_3, m_3}(\theta, \phi) \sigma_3 Y_{l_4, m_4}(\theta', \phi') \sigma_4 \rangle \quad (4.14) \\
& = \sum_{k=0}^{\infty} \sum_{m=-k}^k \sum_{\tau_1, \tau_2, \tau_3, \tau_4} \langle Y_{l_1, m_1}(\theta, \phi) \sigma_1 | Y_{k, m}(\theta, \phi) | Y_{l_3, m_3}(\theta, \phi) \sigma_3 \rangle \\
& \qquad \qquad \qquad \langle Y_{l_2, m_2}(\theta', \phi') \sigma_2 | Y_{k, m}^*(\theta', \phi') | Y_{l_4, m_4}(\theta', \phi') \sigma_4 \rangle .
\end{aligned}$$

We have in (4.14) integrals involving three spherical harmonics which are given by the Gaunt coefficients. This can be used to restrict the values of the summation over k and m . The Gaunt coefficients are different from zero in the first integral only for $m = m_1 - m_3$. Similarly, the second integral is different from zero for $m = m_4 - m_2$. Hence, in combination, one concludes that the total M_z is conserved ($m_1 + m_2 = m_3 + m_4$) for the integrals. Furthermore, the values of k are restricted to values of $k \leq \min(|l_1 + l_4|, |l_2 + l_3|)$. This simplifies the angular part.

Let us now investigate the radial part. The general expression for a scattering event involving four different shells is expressed in (4.15)

$$\sum_{\tau_1, \tau_2, \tau_3, \tau_4} \langle R_{n_1, l_1}(r) R_{n_2, l_2}(r') | \sum_{k=0}^{\min(|l_1+l_4|, |l_2+l_3|)} \frac{r^k}{r^{k+1}} | R_{n_3, l_3}(r) R_{n_4, l_4}(r') \rangle . \quad (4.15)$$

In the case of Coulomb interaction in a single shell, $n_1 = n_2 = n_3 = n_4$ and $l_1 = l_2 = l_3 = l_4$ and hence one obtains the expression

$$F^{(k)} = \sum_{k=0}^{2l} \langle R_{n, l}(r) R_{n, l}(r') | \frac{r^k}{r^{k+1}} | R_{n, l}(r) R_{n, l}(r') \rangle . \quad (4.16)$$

For a $3d^n$ configuration, $2l = 4$ yielding values of $k = 0, 2, 4$ and one has to evaluate three Slater integrals $F^{(k)}$ for such a configuration. For an excited state with a core hole, like the excited state of a L absorption edge with a configuration $2p^5 3d^{n+1}$, it is necessary to take into consideration the Coulomb interaction between the $2p$ and the $3d$ shells. There are two possible cases for these scattering events (see also Chap. 2):

1. Direct interaction with $n_1 = n_3$ and $n_2 = n_4$. This means that each electron scatters in its shell. The matrix elements read

$$F^{(k)} = \sum_{k=0}^{\min(|2l_1, 2l_2|)} \langle R_{n_1, l_1}(r) R_{n_2, l_2}(r') | \frac{r^k}{r^{k+1}} | R_{n_1, l_1}(r) R_{n_2, l_2}(r') \rangle . \quad (4.17)$$

2. Exchange interaction with $n_1 = n_4$ and $n_2 = n_3$. This means that electrons exchange shells. The matrix elements read

$$G^{(k)} = \sum_{k=0}^{\min(|2l_1, 2l_2|)} \langle R_{n_1, l_1}(r) R_{n_2, l_2}(r') | \frac{r^k}{r^{k+1}} | R_{n_2, l_2}(r) R_{n_1, l_1}(r') \rangle. \quad (4.18)$$

The $F^{(k)}$ and $G^{(k)}$ are called Slater integrals. The magnitude of the multiplet splitting depends on the magnitude of the Slater integrals. For an atomic calculation (corresponding to the case of a free ion in spherical symmetry) radial integrals are calculated self-consistently using a Hartree–Fock model, with values typically of the order of a few eV (not more than tens of eV). In the point group symmetry, where the absorber is considered with its environment, these values are reduced empirically in order to take into account the effect of the chemical bond which delocalizes the electrons. This reduction factor is an adjustable parameter (typically, 60–80% for a iono-covalent bond, 100% being the ionic limit case of a free ion).

The Crystal Field Hamiltonian

Let us now extend our theoretical framework to include the effect of the CF potential on the absorbing ion. This is done by considering the N nearest neighbours as point charges ($Z_i e$) at positions \mathbf{R}_i . The electrostatic potential due to these point charges at position \mathbf{r} , $V_{CF}(\mathbf{r})$, is expressed as

$$V_{CF}(\mathbf{r}) = \sum_{i=1}^N \frac{Z_i e^2}{|\mathbf{r} - \mathbf{R}_i|}. \quad (4.19)$$

A multipole expansion of the potential can be used to expand (4.19), leading to the expression

$$V_{CF}(r, \theta, \phi) = e^2 \sum_{k=0}^{\infty} r^k \sum_{m=-k}^k C_{k,m}(\theta, \phi) Q_{k,m}, \quad (4.20)$$

with $Q_{k,m} \equiv \left[\frac{4\pi}{2k+1} \right]^{1/2} \sum_{i=1}^N Z_i \left(\frac{1}{R_i} \right)^{k+1} Y_{k,m}^*(\theta_i, \phi_i)$. $Y_{k,m}$ is the spherical harmonic, $C_{k,m}$ is the renormalized spherical harmonic, and $*$ is the complex conjugate. Note here that one assumes that the radial extent of the $3d$ orbitals is smaller than the distance between the absorbing ion and its first neighbours (i.e., $r \ll R_i$). The CF Hamiltonian can be developed using the single-particle basis (atomic spin-orbitals as discussed before for the Coulomb interaction). Separating the radial and angular parts leads to

$$\hat{H}_{CF} = \sum_{\tau_1, \tau_2} \sum_{k,m} A_{k,m} \langle Y_{\ell_1, m_1} \sigma_1 | C_{k,m} | Y_{\ell_2, m_2} \sigma_2 \rangle c_{\tau_1}^\dagger c_{\tau_2}. \quad (4.21)$$

Here, the $A_{k,m}$ combine all the radial parts of (4.20). They are related to the usual CF parameters ($10Dq$, Ds , Dt , ...) which are usually not known precisely. The CF parameters (or $A_{k,m}$) are either fitted parameters or taken from experiments (optical absorption, electron paramagnetic resonance, ...). It is important to warn the reader against the temptation to fit the calculation with an unreasonable number of CF

parameters: with adjustable parameters, one runs the risk of producing some spectra in good agreement with experiments not for a theoretically justifiable reason but rather due to some lucky cancellation between inappropriate choices of the parameters and inaccurate theoretical approximations employed in solving the model. It is therefore important that one uses some sensible limits for these parameters and critically examines the values used in the model.

Equation 4.21 is a useful expression because the matrix elements are integrals again over three spherical harmonics and are given by the Gaunt coefficients. Furthermore, the series can be truncated according to the triangular condition. For $3d$ orbitals (like in the case of an Fe ion), $\ell_1 = \ell_2 = 2$ so the maximum value of m possible is $m = 4$ with $k \leq 4$. The actual form of the matrix elements depends on the symmetry of the CF potential.

We will present the example of an octahedral (O_h) cluster to illustrate the procedure of calculating the CF matrix elements. In the case of an O_h cluster, six neighbours are positioned at equal distances from the central ion as shown in Fig. 4.1. We will first calculate the multipole terms possible for this configuration according to (4.20). This can be easily evaluated and many softwares are available such as the ‘‘multipoles’’ Python package [8]. One finds that the multipole expansion of the octahedral potential reduces to the following terms with the coefficients listed below $C_{0,0} \rightarrow 6$, $C_{4,0} \rightarrow \sqrt{\frac{49}{4}}$, $C_{4,4} \rightarrow \sqrt{\frac{35}{8}}$, $C_{4,-4} \rightarrow \sqrt{\frac{35}{8}}$.

Now we can evaluate the matrix elements of (4.21) using the Gaunt coefficients. One finds the following matrix for O_h crystal field

$$\sum_{k,m} \langle Y_{2,m_1} | C_{k,m} | Y_{2,m_2} \rangle \propto \begin{bmatrix} 1 & 0 & 0 & 0 & 5 \\ 0 & -4 & 0 & 0 & 0 \\ 0 & 0 & 6 & 0 & 0 \\ 0 & 0 & 0 & -4 & 0 \\ 5 & 0 & 0 & 0 & 1 \end{bmatrix}. \quad (4.22)$$

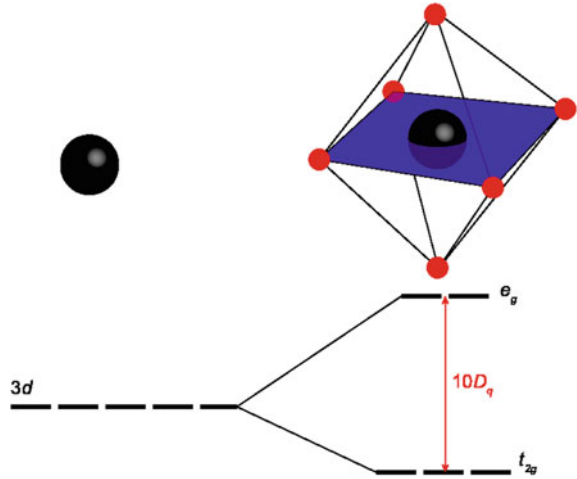
Diagonalizing this matrix gives the following eigenvalues $E = 6, -4, -4, 6, -4$ for the eigenvectors

$$\begin{bmatrix} \frac{1}{\sqrt{2}} \\ 0 \\ 0 \\ 0 \\ \frac{1}{\sqrt{2}} \end{bmatrix}, \begin{bmatrix} -\frac{1}{\sqrt{2}} \\ 0 \\ 0 \\ 0 \\ \frac{1}{\sqrt{2}} \end{bmatrix}, \begin{bmatrix} 0 \\ 1 \\ 0 \\ 0 \\ 0 \end{bmatrix}, \begin{bmatrix} 0 \\ 0 \\ 1 \\ 0 \\ 0 \end{bmatrix}, \begin{bmatrix} 0 \\ 0 \\ 0 \\ 1 \\ 0 \end{bmatrix}. \quad (4.23)$$

This illustrates the splitting of the $3d$ one electron orbitals in an O_h crystal field as shown in Fig. 4.1. The energy difference between the t_{2g} and e_g orbitals is referred to as $10Dq$ and its magnitude depends on the radial part $A_{k,m}$. The five degenerate orbitals split into two types of orbital:

1. Three orbitals of energies $-4Dq$ referred to as the t_{2g} orbitals and which are $\frac{1}{\sqrt{2}}(Y_{2,-2} - Y_{2,2})$, $Y_{2,1}$, and $Y_{2,-1}$.

Fig. 4.1 Splitting of the five degenerate $3d$ orbitals (left) into t_{2g} and e_g orbitals in an octahedral crystal field (right)



- Two orbitals of energies $6Dq$ referred to as the e_g orbitals and which are $\frac{1}{\sqrt{2}}(Y_{2,-2} + Y_{2,2})$, and $Y_{2,0}$.

The same procedure can be used to determine the eigenstates and energies of the $3d$ (or any other) orbitals embedded in a certain symmetry.

4.1.3.3 The Many-Body Extended Picture of Electronic States

The most recently developed approaches aim at extending both DFT and LFM theories to provide a comprehensive description of many-body interactions. An example for a rather manageable improvement to DFT is to add a static Hubbard parameter U to account for on-site electronic repulsion. In addition, there are other approaches that go well beyond DFT. They can be grouped into two main types: the quantum chemistry approaches (mainly, wave function-based methods) and the Green's function methods.

Quantum chemistry approaches (DFT-CI, multi-configurational self consistent field [configuration interaction (CI)], coupled cluster, quantum Monte Carlo) are many-body extended approaches. In DFT-CI, for example, a combination of Slater determinants is used to describe the wave function of the system. The number of configurations that can be considered is limited by computing power and one has to decide which configurations to include. These approaches can only be applied for small clusters and molecules due to computational demand. Green's functions based methods, such as GW and dynamical mean-field theory (DMFT) provide an alternative approach to calculate the electronic structure of strongly correlated materials. In a GW method, a screened Coulomb interaction (W) is calculated following a DFT calculation of the charge density. A nonlocal energy dependent self-energy operator is required. Furthermore, DMFT can be utilized to map the full lattice problem onto

a single site quantum impurity problem, using a local screened Coulomb interaction (U). In both GW and DMFT approaches, correlations (many-body effects) are significantly better described than in standard DFT.

4.1.3.4 Which Approach Works Best for Core Level Spectroscopy Calculations?

Unfortunately this is a very complex question: it depends on the chemical system (ionic, covalent, strongly correlated, ...), the edge (K -, L -edges, ...) and the type of spectroscopy (absorption, photoemission, ...). Consequently, in the following we try to provide some guiding considerations.

A good starting criterion for the choice of the method of calculation is the localization of the final state wave function. When electrons are excited into highly delocalized orbitals, they interact much less with other electrons meaning that the intra-atomic interactions are expected to be small. In this case single-particle approaches often give satisfactory results as the multi-electronic effects are small. This may be the case for the K edge of $3d$ elements and the $L_{2,3}$ edges of heavy elements (e.g., rare earths, $5d$ transition metals), as well as the K edges of ligands (such as C, N, O, S).

On the other hand, when electrons are excited into localized orbitals, they will strongly interact with each other and the core hole. In this case, the multi-electronic effects become significant, and description considering only the absorber atom may be more successful such as LFM theory. This is typically the case for $L_{2,3}$ edges of $3d$ elements and $M_{4,5}$ edges of $4f$ elements.

In intermediate cases where both intra- and inter-atomic effects are relevant, like the K pre-edge of $3d$ elements, single-particle and many-body approaches may work or fail. It may also happen that different energy ranges of a spectrum are best described by different theoretical approaches. This is often the case when a weak pre-edge feature is observed before the strong main edge. The pre-edges often arise from excitations into localized orbitals while the main edge has a more delocalized character. Whether the final state is localized or not may be derived from the shape of the absorption edge. When the edge is dominated by a step function, the final state can be assumed to be delocalized. If it exhibits distinct peaks that decrease sharply, this may be due (but not necessarily) to a localized final state.

4.1.4 Codes for Ligand-Field Multiplet Calculations

Regarding the practical aspects of calculating core level spectra, one faces yet another level of complexity as the plethora of theoretical methods mentioned above are implemented in a comparably large number of computational packages. Instead of trying to provide an overview of all the available computational tools, we will focus on introducing Quanta, one of the currently available software packages that can

be used to perform ligand-field multiplet calculations, and Crispy a graphical user interface that uses Quanty as a computational engine.

Quanty [9–12] is developed by Maurits Haverkort and his collaborators at the Institute of Theoretical Physics at Heidelberg University. It is a computational library that can be used to write quantum mechanical programs in the second quantization formalism. While the library can be used to describe a wide range of problems, it is specifically aimed at calculating different spectroscopies, including core level spectroscopy. Briefly, the user starts by constructing the Hamiltonian for the system of interest, diagonalize it, selects several eigenstates, and then calculates the spectrum corresponding to these eigenstates. In Quanty the Hamiltonian is expressed in a basis of one particle modes, which can be both fermionic and bosonic. The fermionic modes are usually spin-orbitals. In semi-empirical multiplet calculations, the interactions between the spin-orbitals are parametrized using values calculated for isolated atoms, which are afterwards scaled to account for the effect of the surrounding atoms. Alternatively, the parameters can be calculated directly by using for example DFT-based methods [9]. After the diagonalization of the Hamiltonian and the selection of the lowest eigenstates, using, for example, Boltzmann statistics, Quanty can be used to calculate the spectrum. As mentioned previously, this is done using a Green's function approach, thereby avoiding the sum-over-states calculation, which can lead to an important reduction in computational time.

The core of the library is written using the C/C++ programming language for maximum efficiency. The users do not interact directly with this part of the code, but rather with the Lua-based layer that wraps it. To run calculations the users are required to write small programs using the functions defined in Quanty. Doing this in a scripting language such as Lua has the advantage of providing an ideal environment for experimentation, circumventing the limitations of compiled programming languages such as C or C++. While this is indeed very helpful, it is not uncommon for such programs to reach more than a few tens of lines of code, which in itself can be intimidating for the majority of new users. Also, as it is the case for many scientific libraries, because of the flexibility given to the users when writing these programs, it is impossible to check for all the things that might be incorrect. This leads to errors that are difficult to trace even for experienced users.

To help users to more easily perform Quanty calculations, one of us (M. Retegan) has developed a friendly user interface that exposes the library's capabilities for a large part of core level spectroscopies. Crispy [13] was developed using the Python programming language and relies on additional packages from the Python ecosystem. The main window of the application is shown in Fig. 4.2. Using Crispy, the users can quickly adjust the parameters of the calculation, run it, and plot the resulting spectrum without the need of writing any programs. The approach has many advantages for novice users, but even experienced ones can use Crispy to generate a starting program that will become the basis of their calculation. Crispy is a free and open-source program that can be installed on any operating system that has an up-to-date Python distribution. For Windows® and macOS® the program comes in easy to install packages that can be downloaded from the official website, <http://www.esrf.eu/computing/scientific/crispy>.

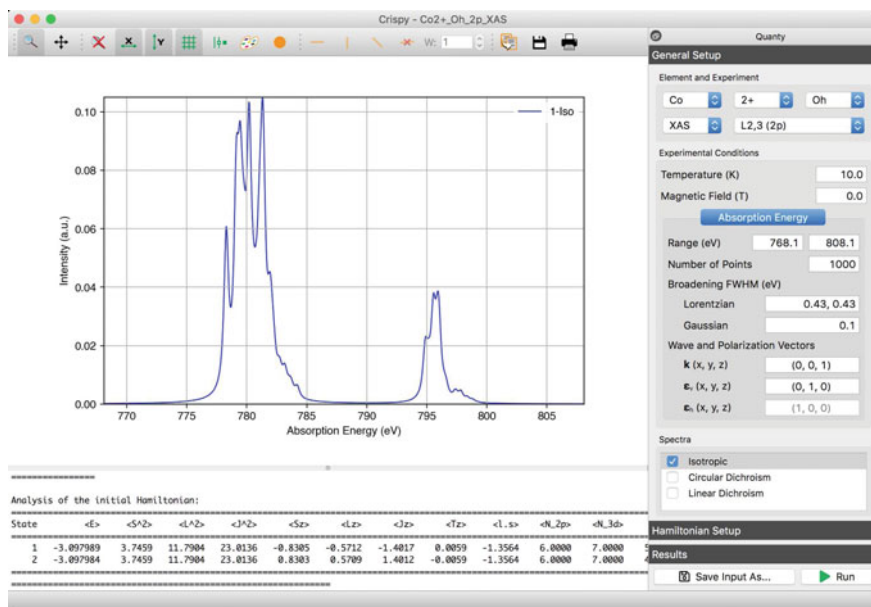


Fig. 4.2 Crispy's main window showing a calculated XAS $L_{2,3}$ spectrum for a Co^{2+} ion in octahedral symmetry

4.2 Spherical Tensor Expansion of the XAS Cross Section

A spherical tensor is a set of components that transform into each others under arbitrary rotations. Another way to state this is to say that the components of a spherical tensor generate a vector space which is invariant under rotation. A spherical tensor is irreducible if this vector space cannot be written as the sum of two invariant (non-zero) subspaces. For an irreducible tensor of rank j , the dimension of the corresponding vector space is $2j + 1$. For example, spherical harmonics $Y_{l,m}$ are the spherical tensor components of a spherical tensor of rank l . Note that while a 3×3 matrix is an irreducible Cartesian tensor, it is a reducible spherical tensor which is the sum of $j = 0$, $j = 1$, and $j = 2$ irreducible spherical tensors. It is evident that such an expansion would provide us with deeper insights by identifying groups of spectra that obey certain symmetry transformation rules which one could easily relate back to the system symmetry [14].

Spherical tensor analysis has been used with great success for the X-ray photoelectron of localized magnetic systems [15–19] and in XAS [14, 20–22], including XNLD [23]. The underlying idea is to determine a finite set of fundamental spectra in terms of which all possible experimental spectra can be expressed. More precisely, the XAS spectrum obtained for a given polarization vector (ϵ) and wave vector (k) of the incident beam is written as a sum of terms which are fundamental spectra [21, 22] (depending only on the sample properties) multiplied by an angular coefficient

depending only on the experimental conditions (\mathbf{k} , $\boldsymbol{\epsilon}$). Such a geometric and fully decoupled expression is useful: (i) to disentangle the properties of the sample from those of the measurement; (ii) to determine specific experimental arrangements aiming at the observation of specific sample properties; (iii) to provide the most convenient starting point to investigate the reduction of the number of fundamental spectra due to crystal symmetries.

4.2.1 The Case of Electric Dipole Transitions

The first step is to build rank one spherical tensors from the vectors appearing in the transition operator. The polarization vector $\boldsymbol{\epsilon} = [\epsilon_x, \epsilon_y, \epsilon_z]$ can be written as a spherical tensor $\boldsymbol{\epsilon}^1$ with components $\epsilon_{-1}^1 = \frac{\epsilon_x - i\epsilon_y}{\sqrt{2}}$, $\epsilon_1^1 = -\frac{\epsilon_x + i\epsilon_y}{\sqrt{2}}$, and $\epsilon_0^1 = \epsilon_z$. Similarly, the position spherical tensor, \mathbf{r}^1 , can be constructed. In the following we shall use the following notation for the coupling of spherical tensors \mathbf{P}^a and \mathbf{Q}^b of ranks a and b into a spherical tensor of rank c

$$\{\mathbf{P}^a \otimes \mathbf{Q}^b\}_\gamma^c = \sum_{\alpha=-a}^a \sum_{\alpha=-b}^b (a\alpha b\beta | c\gamma) P_\alpha^a Q_\beta^b, \quad (4.24)$$

with $(a\alpha b\beta | c\gamma)$ being the Clebsch–Gordan coefficients. Therefore,

$$\mathbf{P}^a \cdot \mathbf{Q}^a = \sum_{\alpha=-a}^a (-1)^\alpha P_{-\alpha}^a Q_\alpha^a = (-1)^a \sqrt{2a+1} \{\mathbf{P}^a \otimes \mathbf{Q}^a\}^0. \quad (4.25)$$

One has now to compute the scalar product of both tensors which is given by (4.25). The dipole transition operator can be written as in (4.26) taking into consideration that \mathbf{r} is real while $\boldsymbol{\epsilon}$ is in general complex

$$\begin{aligned} T &= -\sqrt{3} \{\boldsymbol{\epsilon}^1 \otimes \mathbf{r}^1\}^0 \\ T^\dagger &= -\sqrt{3} \{\boldsymbol{\epsilon}^{1*} \otimes \mathbf{r}^1\}^0. \end{aligned} \quad (4.26)$$

We can recouple the cross section such that polarization tensors are coupled to each other and position tensors are coupled to each other. This means that the expression will have a part that depends only on the experimental geometry (polarization vector) and a part that depends only on the sample properties. This recoupling can be done using the identity

$$\{\mathbf{P}^g \otimes \mathbf{Q}^g\}^0 \cdot \{\mathbf{R}^d \otimes \mathbf{S}^d\}^0 = \sum_a (-1)^a \frac{\{\mathbf{P}^g \otimes \mathbf{R}^d\}^a \cdot \{\mathbf{Q}^g \otimes \mathbf{S}^d\}^a}{\sqrt{(2g+1)(2d+1)}}. \quad (4.27)$$

Here a is constrained to $|g - d| \leq a \leq g + d$. Hence, for the dipole transition, $g = d = 1$ and $0 \leq a \leq 2$. The recoupled XAS cross section is finally expressed as follows:

$$\sigma_\omega = -4\pi\alpha\hbar\omega \text{Im} \left[\sum_{a=0}^2 (-1)^a \{\epsilon^{1*} \otimes \epsilon^1\}^a \cdot \{\langle I|r^1 G^+ r^1|I\rangle\}^a \right]. \quad (4.28)$$

Quanty can calculate the energy dependent tensors $R^{(a)} = \{\langle I|r^1 G^+ r^1|I\rangle\}^a$ that depend only on the properties of the sample. We will refer to these elements as the fundamental spectra. Note that these fundamental spectra are sometimes referred to as $\sigma^{(a)}$. This could be confused with the total cross section σ_ω so we shall not use this notation here. The experimental geometry tensor is $E^a = \{\epsilon^{1*} \otimes \epsilon^1\}^a$.

4.2.1.1 Term $a = 0$

The first term can be found by substituting $a = 0$ in (4.28). This is the zero rank of the tensor, given in (4.29).

$$\begin{aligned} \sigma(0, 0) = 4\pi\alpha\hbar\omega \times \text{Im} \left[\frac{1}{3} \left(\langle I|rC_{1,0}^* G^+ rC_{1,0}|I\rangle + \langle I|rC_{1,-1}^* G^+ rC_{1,-1}|I\rangle \right. \right. \\ \left. \left. + \langle I|rC_{1,1}^* G^+ rC_{1,1}|I\rangle \right) \right]. \end{aligned} \quad (4.29)$$

Here $C_{\ell m} = C_m^\ell = \sqrt{\frac{4\pi}{2\ell+1}} Y_\ell^m$. The term $\sigma(0, 0)$ is independent of the incident polarization vector and as such is rotation invariant. It gives the isotropic contribution of the XAS cross section.

4.2.1.2 Term $a = 1$

The term $a = 1$ consists of three components, namely, $\sigma(1, 0)$, $\sigma(1, 1)$, and $\sigma(1, -1)$:

$$\begin{aligned} \sigma(1, 0) = -4\pi\alpha\hbar\omega \times \text{Im} \left[\frac{1}{2} \left(i\epsilon_x^* \epsilon_y - i\epsilon_x \epsilon_y^* \right) \right. \\ \left. \times \left(\langle I|rC_{1,1}^* G^+ rC_{1,1}|I\rangle - \langle I|rC_{1,-1}^* G^+ rC_{1,-1}|I\rangle \right) \right], \end{aligned} \quad (4.30)$$

$$\sigma(1, 1) = -4\pi\alpha\hbar\omega \times \text{Im} \left[\frac{-1}{2\sqrt{2}} \left(\epsilon_x^* \epsilon_z - \epsilon_x \epsilon_z^* + i\epsilon_y \epsilon_z^* - i\epsilon_y^* \epsilon_z \right) \right] \quad (4.31)$$

$$\left(\langle I|rC_{1,0}^*G^+rC_{1,1}|I \rangle + \langle I|rC_{1,-1}^*G^+rC_{1,0}|I \rangle \right) \Big], \quad (4.32)$$

$$\sigma(1, -1) = -4\pi\alpha\hbar\omega \times \text{Im} \left[\frac{1}{2\sqrt{2}} \left(\epsilon_x^* \epsilon_z - \epsilon_x \epsilon_z^* + i\epsilon_y^* \epsilon_z - i\epsilon_y \epsilon_z^* \right) \right. \\ \left. \times \left(\langle I|rC_{1,0}^*G^+rC_{1,-1}|I \rangle + \langle I|rC_{1,1}^*G^+rC_{1,0}|I \rangle \right) \right]. \quad (4.33)$$

One notices from (4.30), (4.32) and (4.33) that the spectra of $a = 1$ are not active if any of these two cases are satisfied:

1. If linearly polarized light is used for the measurement.
2. If all off-diagonal elements are zero and the diagonal elements are equal.

Another conclusion that can be drawn from the recoupling is the necessity to perform XAS measurements using both linearly and circularly polarized light to probe these fundamental spectra.

4.2.1.3 Term $a = 2$

The term $a = 2$ consists of five components, namely, $\sigma(2, 0)$, $\sigma(2, 1)$, $\sigma(2, -1)$, $\sigma(2, 2)$, and $\sigma(2, -2)$. These are given below as follows:

$$\sigma(2, 0) = -4\pi\alpha\hbar\omega \times \text{Im} \left[\frac{1}{6} \left(2|\epsilon_z|^2 - |\epsilon_x|^2 - |\epsilon_y|^2 \right) \left(2\langle I|rC_{1,0}^*G^+rC_{1,0}|I \rangle \right. \right. \\ \left. \left. - \langle I|rC_{1,-1}^*G^+rC_{1,-1}|I \rangle - \langle I|rC_{1,1}^*G^+rC_{1,1}|I \rangle \right) \right], \quad (4.34)$$

$$\sigma(2, 1) = -4\pi\alpha\hbar\omega \times \text{Im} \left[\frac{1}{2\sqrt{2}} \left(\epsilon_x \epsilon_z^* + \epsilon_x^* \epsilon_z - i\epsilon_y \epsilon_z^* - i\epsilon_y^* \epsilon_z \right) \right. \\ \left. \times \left(\langle I|rC_{1,-1}^*G^+rC_{1,0}|I \rangle - \langle I|rC_{1,0}^*G^+rC_{1,1}|I \rangle \right) \right], \quad (4.35)$$

$$\sigma(2, -1) = -4\pi\alpha\hbar\omega \times \text{Im} \left[\frac{1}{2\sqrt{2}} \left(\epsilon_x \epsilon_z^* + \epsilon_x^* \epsilon_z + i\epsilon_y^* \epsilon_z + i\epsilon_y \epsilon_z^* \right) \right. \\ \left. \times \left(\langle I|rC_{1,0}^*G^+rC_{1,-1}|I \rangle - \langle I|rC_{1,1}^*G^+rC_{1,0}|I \rangle \right) \right], \quad (4.36)$$

$$\begin{aligned} \sigma(2, 2) = & -4\pi\alpha\hbar\omega \times \text{Im} \left[\frac{-1}{2} \left((\epsilon_x - i\epsilon_y)(\epsilon_x^* - i\epsilon_y^*) \right) \right. \\ & \left. \times \left(\langle I | r C_{1,-1}^* G^+ r C_{1,1} | I \rangle \right) \right], \end{aligned} \quad (4.37)$$

$$\begin{aligned} \sigma(2, -2) = & -4\pi\alpha\hbar\omega \times \text{Im} \left[\frac{-1}{2} \left((\epsilon_x + i\epsilon_y)(\epsilon_x^* + i\epsilon_y^*) \right) \right. \\ & \left. \times \left(\langle I | r C_{1,1}^* G^+ r C_{1,-1} | I \rangle \right) \right]. \end{aligned} \quad (4.38)$$

It can be noted from (4.34), (4.35), (4.36), (4.37), and (4.38) that the $a = 2$ spectra are active for linearly polarized light and hence these spectra are responsible for the angular dependence observed with linear light. On the contrary, no difference can be observed between right and left circularly polarized light. Another feature of these terms is that they are not active if the following two conditions are satisfied:

1. The diagonal matrix elements are equal.
2. The off-diagonal matrix elements are zero.

4.2.1.4 General Dipole Expression

The general dipole expression is given in (4.39). From this equation, the dipole XAS cross-section for an arbitrary polarization (ϵ) can be constructed from the nine fundamental spectra derived above.

$$\begin{aligned} \sigma_{\omega}^{Dipole}(\epsilon) = & -4\pi\alpha\hbar\omega \times \text{Im} \left[\frac{1}{3} R(0, 0) + \frac{1}{2} (i\epsilon_x^* \epsilon_y - i\epsilon_x \epsilon_y^*) R(1, 0) \right. \\ & - \frac{1}{2\sqrt{2}} (\epsilon_x^* \epsilon_z - \epsilon_x \epsilon_z^* + i\epsilon_y \epsilon_z^* - i\epsilon_y^* \epsilon_z) R(1, 1) \\ & + \frac{1}{2\sqrt{2}} (\epsilon_x^* \epsilon_z - \epsilon_x \epsilon_z^* + i\epsilon_y^* \epsilon_z - i\epsilon_y \epsilon_z^*) R(1, -1) \\ & + \frac{1}{6} (2|\epsilon_z|^2 - |\epsilon_x|^2 - |\epsilon_y|^2) R(2, 0) \\ & + \frac{1}{2\sqrt{2}} (\epsilon_x \epsilon_z^* + \epsilon_x^* \epsilon_z - i\epsilon_y \epsilon_z^* - i\epsilon_y^* \epsilon_z) R(2, 1) \\ & + \frac{1}{2\sqrt{2}} (\epsilon_x \epsilon_z^* + \epsilon_x^* \epsilon_z + i\epsilon_y^* \epsilon_z + i\epsilon_y \epsilon_z^*) R(2, -1) \\ & - \frac{1}{2} ((\epsilon_x - i\epsilon_y)(\epsilon_x^* - i\epsilon_y^*)) R(2, 2) \\ & \left. - \frac{1}{2} ((\epsilon_x + i\epsilon_y)(\epsilon_x^* + i\epsilon_y^*)) R(2, -2) \right], \end{aligned} \quad (4.39)$$

where the R are the fundamental spectra and are defined as

$$R(0, 0) = \langle I|rC_{1,0}^*G^+rC_{1,0}|I \rangle + \langle I|rC_{1,-1}^*G^+rC_{1,-1}^1|I \rangle \\ + \langle I|rC_{1,1}^1G^+rC_{1,1}|I \rangle, \quad (4.40)$$

$$R(1, 0) = \langle I|rC_{1,1}^*G^+rC_{1,1}|I \rangle - \langle I|rC_{1,-1}^*G^+rC_{1,-1}|I \rangle, \quad (4.41)$$

$$R(1, 1) = \langle I|rC_{1,0}^*G^+rC_{1,1}|I \rangle + \langle I|rC_{1,-1}^*G^+rC_{1,0}|I \rangle, \quad (4.42)$$

$$R(1, -1) = \langle I|rC_{1,0}^*G^+rC_{1,-1}|I \rangle + \langle I|rC_{1,1}^*G^+rC_{1,0}|I \rangle, \quad (4.43)$$

$$R(2, 0) = 2\langle I|rC_{1,0}^*G^+rC_{1,0}|I \rangle - \langle I|rC_{1,-1}^*G^+rC_{1,-1}|I \rangle \\ - \langle I|rC_{1,1}^*G^+rC_{1,1}|I \rangle, \quad (4.44)$$

$$R(2, 1) = \langle I|rC_{1,-1}^*G^+rC_{1,0}|I \rangle - \langle I|rC_{1,0}^*G^+rC_{1,1}|I \rangle, \quad (4.45)$$

$$R(2, -1) = \langle I|rC_{1,0}^*G^+rC_{1,-1}|I \rangle - \langle I|rC_{1,1}^*G^+rC_{1,0}|I \rangle, \quad (4.46)$$

$$R(2, 2) = \langle I|rC_{1,-1}^*G^+rC_{1,1}|I \rangle, \quad (4.47)$$

$$R(2, -2) = \langle I|rC_{1,1}^*G^+rC_{1,-1}|I \rangle. \quad (4.48)$$

4.2.1.5 Case Study of a d^9 ion

Octahedral Crystal Field

Equation (4.39) can be simplified when the symmetry of the absorbing system is taken into account. As a demonstration, we shall study a d^9 ion in octahedral (O_h) symmetry. Figure 4.3 (top) shows the matrix elements for such a system. These matrix elements are the direct output of Quanyt and will be referred to as the conductivity tensor. One finds that all the off-diagonal matrix elements are equal to zero and all the diagonal matrix elements are equal. This leaves only the $R(0, 0)$ term of (4.39) not equal to zero. Hence one can conclude that the cross section of a dipole transition is isotropic in an O_h system.

Tetragonal Crystal Field

Let us now consider a tetragonal distortion such that the octahedron is compressed along the z -axis. The ground state in this case has a hole in the d_{z^2} orbital (neglecting spin-orbit coupling) and the z -axis is now different from the x - and y -axes. The conductivity tensor for such a system is shown in Fig. 4.3 (bottom). As could be intuitively expected, the middle panel corresponding to $C_0^1G^+C_0^1$ is different from the other two diagonal elements. This implies that the following terms come into play (see Fig. 4.4):

- $R(0, 0)$ which gives the isotropic cross section.
- $R(2, 0)$ which has a polarization dependence of the form $\frac{1}{6}(2|\epsilon_z|^2 - |\epsilon_x|^2 - |\epsilon_y|^2)$.

It is interesting in this case to investigate what types of dichroism effect could be observed. Consider rotating the incident linear polarization vector in the $x - y$ -plane.

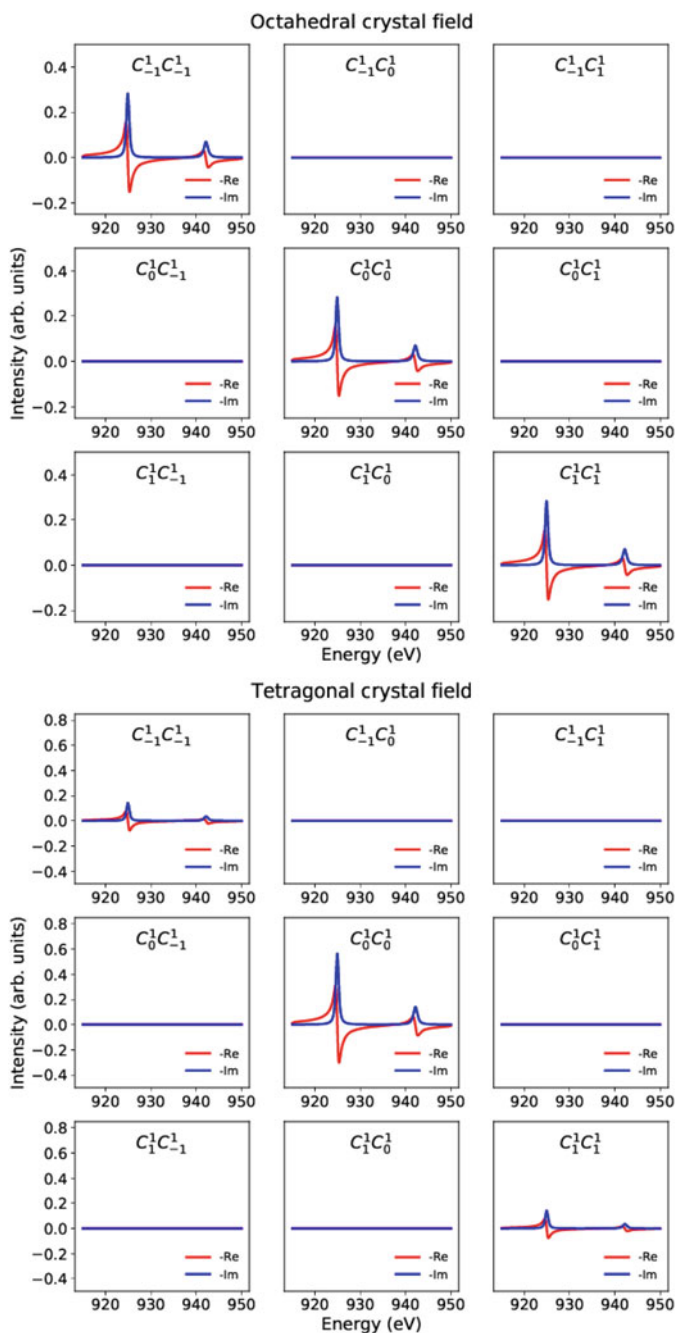


Fig. 4.3 Conductivity tensor calculated for a d^9 ion in an octahedral crystal field (top) and in a tetragonal crystal field (bottom). Calculations are done with a crystal field parameter $10D_q = 1.1$ eV and with $D_s = -0.2$ eV in tetragonal symmetry. Re and Im are the real and imaginary parts of the tensor

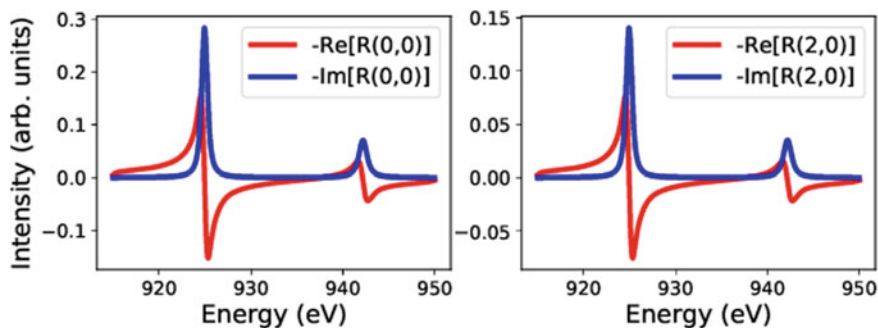


Fig. 4.4 Fundamental spectra $R(0, 0)$ and $R(2, 0)$ for a dipole transition for a d^9 ion in a tetragonal crystal field ($10D_q = 1.1$ eV and $D_s = -0.2$ eV)

In this case $\epsilon = [\cos(\theta), \sin(\theta), 0]$ where θ is the rotation angle defined from the x -axis. The expression of the polarization dependence for the term $R(2, 0)$ reveals that no angular dependence is to be expected in this case. The system is effectively O_h in the $x - y$ -plane and one would expect no angular dependence as discussed in the previous example. This XAS cross section for this rotation is shown in Fig. 4.5a. On the contrary, rotating the polarization vector in the $x - z$ ($\epsilon = [\cos(\theta), 0, \sin(\theta)]$) or $y - z$ ($\epsilon = [0, \cos(\theta), \sin(\theta)]$) planes should yield an angular dependence as the polarization vector probes the distortion, which is indeed observed as shown in Fig. 4.5b and c. The dependence of the XAS cross-section on the direction of the

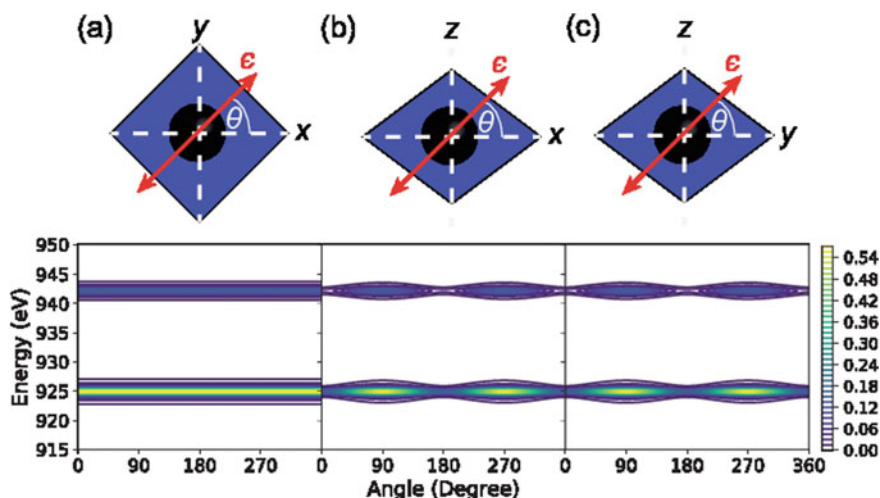


Fig. 4.5 Angular dependence of the $L_{2,3}$ XAS of a $3d^9$ ion in a tetragonal crystal field. Calculations are done by rotating the polarization vector in the $x - y$ -plane [panel (a)], $x - z$ -plane [panel (b)], and $y - z$ -plane [panel (c)] as illustrated in the top panel

linearly polarized light is an effect referred to as linear dichroism as discussed previously.

Octahedral Crystal Field with an Exchange Field $\parallel z$

Another interesting system to investigate is a magnetic $3d^9$ ion where the crystal field is O_h with an exchange field aligned along the z -axis. Hence, the z -axis is inequivalent to the x - and y -axes due to the exchange field. The conductivity tensor of such a system is shown in Fig. 4.6. The exchange field is aligned along a high symmetry direction in this example which preserves the C_4 rotation symmetry of the system and consequently preserves the symmetry of the conductivity tensor. All off-diagonal elements are zero. Note that the off-diagonal elements are zero because we chose to calculate the tensor using the symmetry adapted transition operators. Three fundamental spectra come into play and are plotted in Fig. 4.7:

- $R(0, 0)$ which gives the isotropic cross section,
- $R(1, 0)$ which has a polarization dependence of the form $\frac{1}{2} (i\epsilon_x^* \epsilon_y - i\epsilon_x \epsilon_y^*)$,
- $R(2, 0)$ which has a polarization dependence of the form $\frac{1}{6} (2|\epsilon_z|^2 - |\epsilon_x|^2 - |\epsilon_y|^2)$.

Nearly no angular dependence can be observed by rotating the incident linear polarization vector in the $x - y$ -, $x - z$ -, and $y - z$ -planes (see Fig. 4.8a, b, and c). This is consistent with the fact that the fundamental spectrum $R(2, 0)$ responsible for the angular dependence is nearly zero [$R(2, 0)$ is about two orders of magnitude smaller than the other two fundamental spectra in this system]. The difference in the absorption cross section of linear polarized light in a magnetic system is an effect referred to as XMLD [24]. The magnitude of the XMLD effect for this system can be seen in Fig. 4.9. Note that the magnitude of the XMLD effect in Fe_3O_4 is $\sim 1\%$ of the XAS signal, which could be reliably measured on existing beamlines [25].

A strong dichroism is observed when circularly polarized light is used as in the case for Fig. 4.10a. Here the incident polarization vector is either left or right polarized about the z -axis leading to a difference in the absorption. This is an effect referred to as X-ray magnetic circular dichroism (XMCD) [26]. It can be seen from the expression of the polarization part of the cross-section that if the incident wave vector is aligned perpendicular to the exchange field, for example, for $\epsilon = [0, -\frac{i}{\sqrt{2}}, \frac{1}{\sqrt{2}}]$, and $\epsilon = [0, -\frac{i}{\sqrt{2}}, -\frac{1}{\sqrt{2}}]$, no XMCD effect is observed. This is shown in Fig. 4.10b and c. This dichroism can be used to quantify the ground state spin and orbital moments of the system as given by the sum rules [27].

Octahedral Crystal Field with an Exchange Field $\parallel [210]$

As a last example, we consider a system in C_1 symmetry. Consider aligning the exchange field along a low symmetry direction, e.g., $[210]$. The exchange field now completely breaks the symmetry of the system and the conductivity tensor has off-diagonal elements (bottom of Fig. 4.6). Contrary to the previous case (where the exchange field was aligned to the z -axis), it is now not possible to find a rotated

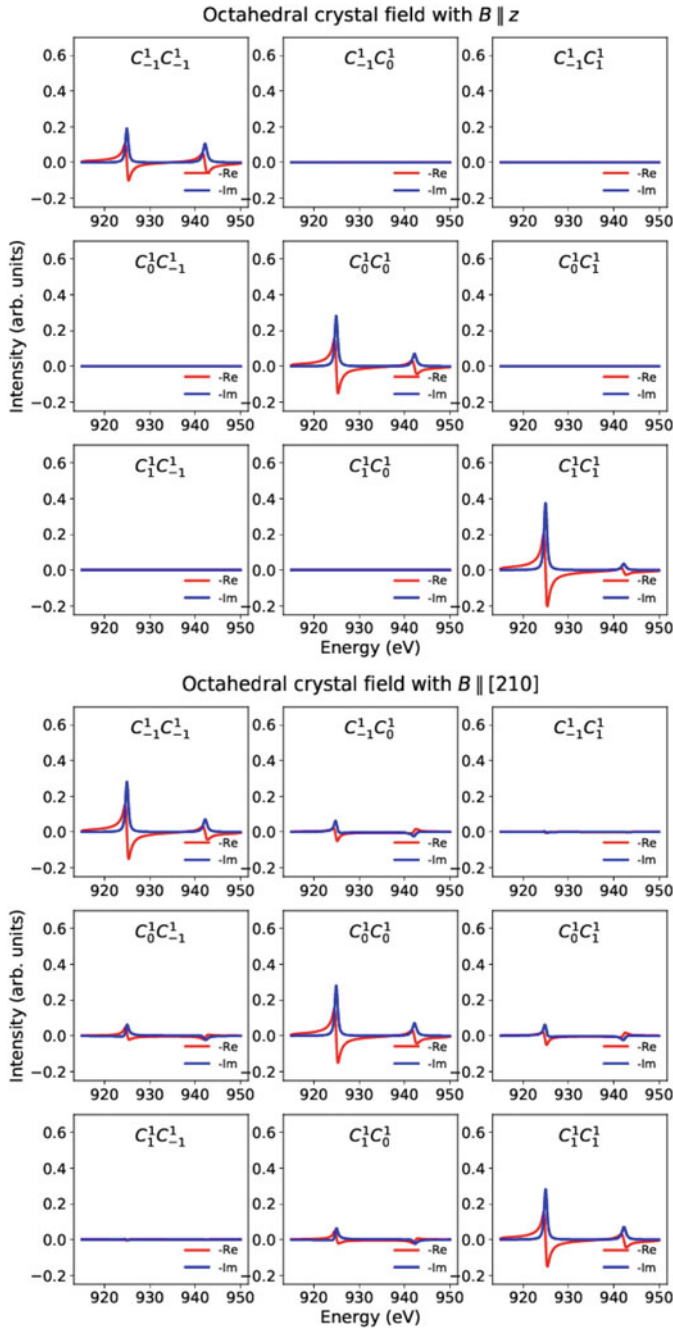


Fig. 4.6 Conductivity tensor calculated for a d^9 ion in an octahedral crystal field ($10D_q = 1.1$ eV) with an exchange field ($B = 0.05$ eV) along the z -axis (top) and along the $[210]$ direction (bottom). The calculations are performed using a real spherical harmonics basis set

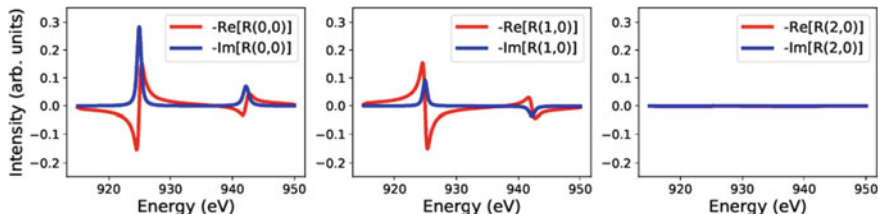


Fig. 4.7 Fundamental spectra $R(0, 0)$, $R(1, 0)$, and $R(2, 0)$ for a dipole transition for a d^9 ion in an octahedral crystal field ($10D_q = 1.1$ eV) with an exchange field ($B = 0.05$ eV) aligned along the z -axis of the cluster

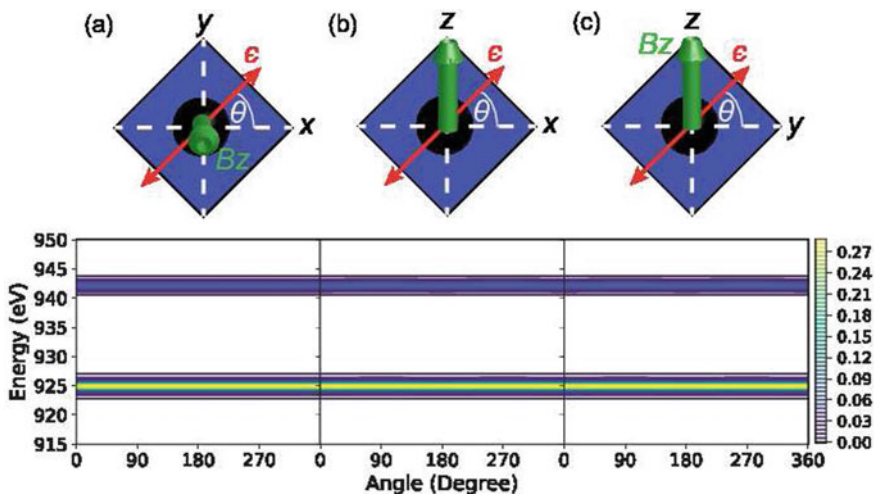


Fig. 4.8 Angular behaviour of the $L_{2,3}$ XAS of a $3d^9$ ion in an octahedral crystal field ($10D_q = 1.1$ eV) with the exchange field ($B_z = 0.05$ eV) aligned along the z -axis. The calculations are done by rotating the polarization vector in the **a** $x - y$ -plane, **b** $x - z$ -plane and **c** $y - z$ -plane as depicted in the top panel

basis set that diagonalizes the conductivity tensor for all excited states (i.e., the basis set becomes energy dependent). It remains possible to diagonalize the conductivity tensor for a given excited state. It is important to realize that when the exchange field is aligned along a low symmetry direction, off-diagonal elements become important and more dichroic effects come into play according to (4.39) and (4.48).

4.2.2 The Case of Electric Quadrupole Transitions

For electric quadrupole transitions, we will follow the same procedure as the one used for electric dipole. The transition operator is now (up to a factor of $i/2$) $T =$

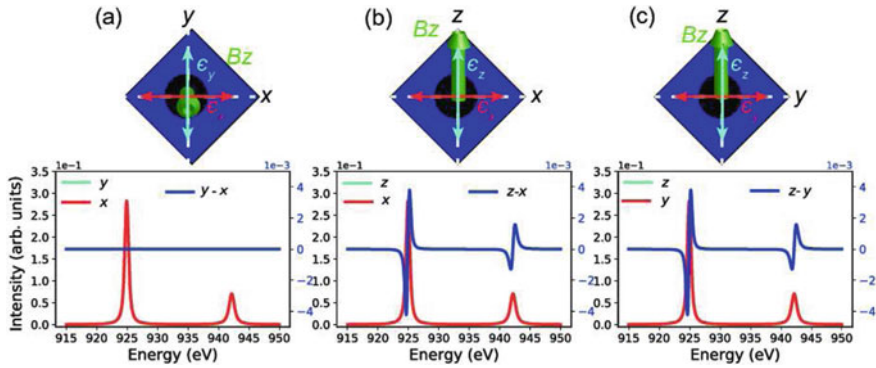


Fig. 4.9 X-ray magnetic linear dichroism of a $3d^9$ ion in an octahedral crystal field ($10D_q = 1.1$ eV) with the exchange field ($B_z = 0.05$ eV) aligned along the z -axis. The dichroism is computed by subtracting the XAS: **a** with $\epsilon \parallel x$ from that with $\epsilon \parallel y$, **b** with $\epsilon \parallel x$ from that with $\epsilon \parallel z$ and **c** with $\epsilon \parallel y$ from that with $\epsilon \parallel z$

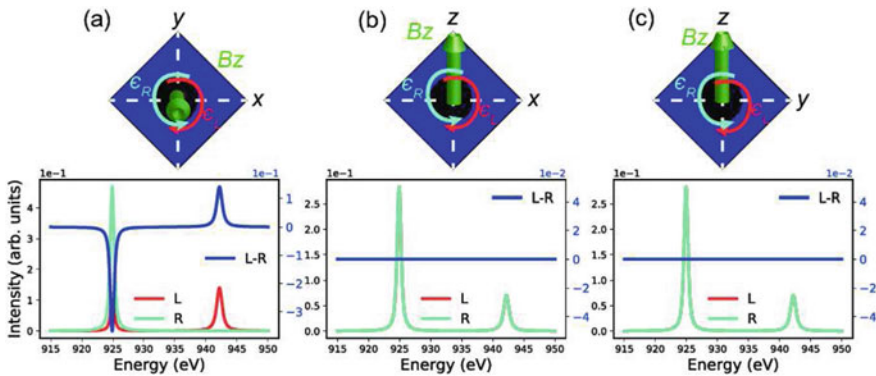


Fig. 4.10 X-ray magnetic circular dichroism of a $3d^9$ ion in an octahedral surrounding with the exchange field (B_z) aligned along the z -axis. The dichroism is computed by subtracting the XAS signal calculated with right circularly polarized light from that with left polarized light. **a** The incident wave vector is aligned parallel to the z -axis. **b** The incident wave vector is aligned parallel to the y -axis. **c** The incident wave vector is aligned parallel to the x -axis

$(\epsilon \cdot r)(\mathbf{k} \cdot r)$. It can be seen from the expression of the transition operator that the cross section will depend on the orientation of the polarization vector (ϵ) and of the wave vector (\mathbf{k}) with respect to the absorbing system. Two recoupling steps are required in this case. First, the transition operator can be rewritten into a combination of scalar products of two tensors: one tensor that depends only on ϵ and \mathbf{k} coupled together, and one tensor that depends only on the absorber \mathbf{r} . This recoupled transition operator is expressed as follows:

$$\begin{aligned}\hat{T} &= \sum_{b=0}^2 (-1)^b \{\boldsymbol{\epsilon}^1 \otimes \mathbf{k}^1\}^b \cdot \{\mathbf{r}^1 \otimes \mathbf{r}^1\}^b, \\ \hat{T}^\dagger &= \sum_{c=0}^2 (-1)^c \{\boldsymbol{\epsilon}^{1*} \otimes \mathbf{k}^1\}^c \cdot \{\mathbf{r}^1 \otimes \mathbf{r}^1\}^c.\end{aligned}\quad (4.49)$$

The next step is to recouple the two transition amplitudes of the absorption cross section. This gives the expression

$$\begin{aligned}\sigma_\omega &= \pi^2 \alpha \hbar \omega \times \text{Im} \left[\sum_{a=0}^4 \sum_{b=0}^2 \sum_{c=0}^2 (-1)^a (-1)^b (-1)^c \{ \{\boldsymbol{\epsilon}^{*1} \otimes \mathbf{k}^1\}^c \otimes \{\boldsymbol{\epsilon}^1 \otimes \mathbf{k}^1\}^b \}^a \right. \\ &\quad \left. \times \{ \langle I | \{\mathbf{r}^1 \otimes \mathbf{r}^1\}^c G^+ \{\mathbf{r}^1 \otimes \mathbf{r}^1\}^b | I \rangle \}^a \right].\end{aligned}\quad (4.50)$$

Before attempting to write out the recoupled absorption cross section in (4.50), it is useful to simplify the expression of the transition operator first. This in turn will simplify the expression of the absorption cross section. The transition operator is a rank two tensor according to (4.49) with $b = 0, 1, 2$. We shall write out the three b terms:

- **Term $b = 0$**

$$\begin{aligned}(-1)^0 \{\boldsymbol{\epsilon}^1 \otimes \mathbf{k}^1\}^0 \cdot \{\mathbf{r}^1 \otimes \mathbf{r}^1\}^0 &= \left(-\frac{1}{\sqrt{3}} \epsilon_0^1 k_0^1 + \frac{1}{\sqrt{3}} \epsilon_1^1 k_{-1}^1 + \frac{1}{\sqrt{3}} \epsilon_{-1}^1 k_1^1 \right) \\ &\quad \times \left(-\frac{1}{\sqrt{3}} r_0^1 r_0^1 + \frac{1}{\sqrt{3}} r_1^1 r_{-1}^1 + \frac{1}{\sqrt{3}} r_{-1}^1 r_1^1 \right)\end{aligned}\quad (4.51)$$

The first part of the expression can be rewritten as $\frac{1}{\sqrt{3}} (-\epsilon_z k_z - \epsilon_x k_x - \epsilon_y k_y)$. This is equal to zero because the polarization vector is orthogonal to the wave vector. This means that the term $b = 0$ is zero.

- **Term $b = 1$**

This term consists of three components according to

$$(-1)^1 \{\boldsymbol{\epsilon}^1 \otimes \mathbf{k}^1\}^1 \cdot \{\mathbf{r}^1 \otimes \mathbf{r}^1\}^1 = -\frac{i}{\sqrt{2}} \frac{i}{\sqrt{2}} (\boldsymbol{\epsilon} \times \mathbf{k}) \cdot (\mathbf{r} \times \mathbf{r}).\quad (4.52)$$

The second part of the expression is equal to zero because it is a cross product of the same vector. This means that the term $b = 1$ is also zero.

- **Term $b = 2$**

This term consists of five components. These five components can be simplified applying the orthogonality between $\boldsymbol{\epsilon}$ and \mathbf{k} . In addition the \mathbf{r} tensor can be expressed in terms of spherical harmonics of $l = 2$ according to the relation

$\{\mathbf{r}^1 \otimes \mathbf{r}^1\}_m^2 = r_m^2 = \sqrt{\frac{8\pi}{15}} Y_{2,m}(\mathbf{r}) = \sqrt{\frac{8\pi}{15}} r^2 Y_{2,m}(\theta, \phi)$. One obtains the following five components after simplification

$$\{\boldsymbol{\epsilon}^1 \otimes \mathbf{k}^1\}_0^2 \{\mathbf{r}^1 \otimes \mathbf{r}^1\}_0^2 = \left(\sqrt{\frac{3}{2}} \epsilon_z k_z \right) (r_0^2), \quad (4.53)$$

$$\{\boldsymbol{\epsilon}^1 \otimes \mathbf{k}^1\}_1^2 \{\mathbf{r}^1 \otimes \mathbf{r}^1\}_{-1}^2 = \left(-\frac{k_z(\epsilon_x + i\epsilon_y) + (k_x + ik_y)\epsilon_z}{2} \right) (r_{-1}^2), \quad (4.54)$$

$$\{\boldsymbol{\epsilon}^1 \otimes \mathbf{k}^1\}_{-1}^2 \{\mathbf{r}^1 \otimes \mathbf{r}^1\}_1^2 = \left(\frac{k_z(\epsilon_x - i\epsilon_y) + (k_x - ik_y)\epsilon_z}{2} \right) (r_1^2), \quad (4.55)$$

$$\{\boldsymbol{\epsilon}^1 \otimes \mathbf{k}^1\}_2^2 \{\mathbf{r}^1 \otimes \mathbf{r}^1\}_{-2}^2 = \left(\frac{(k_x + ik_y)(\epsilon_x + i\epsilon_y)}{2} \right) (r_{-2}^2), \quad (4.56)$$

$$\{\boldsymbol{\epsilon}^1 \otimes \mathbf{k}^1\}_{-2}^2 \{\mathbf{r}^1 \otimes \mathbf{r}^1\}_2^2 = \left(\frac{(k_x - ik_y)(\epsilon_x - i\epsilon_y)}{2} \right) (r_2^2). \quad (4.57)$$

The same arguments apply for the $c = 0, 1, 2$ terms of the recoupled \hat{T}^\dagger operator ending up with the values $b = 2$ and $c = 2$ for the XAS cross section. The recoupled cross section writes

$$\begin{aligned} \sigma_\omega = \pi^2 \alpha \hbar \omega k^2 \times \text{Im} \left[\sum_{a=0}^4 (-1)^a \{ \{\boldsymbol{\epsilon}^{*1} \otimes \mathbf{k}^1\}^2 \otimes \{\boldsymbol{\epsilon}^1 \otimes \mathbf{k}^1\}^2 \}^a \right. \\ \left. \times \{ \langle I | \{\mathbf{r}^1 \otimes \mathbf{r}^1\}^2 G^+ \{\mathbf{r}^1 \otimes \mathbf{r}^1\}^2 | I \rangle \}^a \right]. \quad (4.58) \end{aligned}$$

Now one can develop (4.58) in further details for $a = 0, 1, 2, 3, 4$. We shall only report the final expression here.

4.2.3 Term $a = 0$

Let us substitute $a = 0$ in (4.58). This is the zero rank of the tensor, $\sigma(0, 0)$, describing an isotropic spectrum

$$\begin{aligned} \sigma(0, 0) = \pi^2 \alpha \hbar \omega k^2 \times \text{Im} \left[\frac{1}{10} \left(\langle I | r^2 C_{2,0}^* G^+ r^2 C_{2,0} | I \rangle + \langle I | r^2 C_{2,-1}^* G^+ r^2 C_{2,-1} | I \rangle \right. \right. \\ \left. \left. + \langle I | r^2 C_{2,1}^* G^+ r^2 C_{2,1} | I \rangle + \langle I | r^2 C_{2,-2}^* G^+ r^2 C_{2,-2} | I \rangle \right. \right. \\ \left. \left. + \langle I | r^2 C_{2,2}^* G^+ r^2 C_{2,2} | I \rangle \right) \right]. \quad (4.59) \end{aligned}$$

4.2.4 Term $a = 1$

The term $a = 1$ consists of three components, namely, $\sigma(1, 0)$, $\sigma(1, 1)$ and $\sigma(1, -1)$

$$\begin{aligned} \sigma(1, 0) = \pi^2 \alpha \hbar \omega k^2 \times \text{Im} \left[\frac{i}{20} \left((2k_x^2 + 2k_y^2 + k_z^2) \epsilon_x \epsilon_x^* - (2k_x^2 + 2k_y^2 + k_z^2) \epsilon_x^* \epsilon_y \right. \right. \\ \left. \left. + k_y k_z \epsilon_x \epsilon_z^* - k_y k_z \epsilon_x^* \epsilon_z + k_x k_z \epsilon_z \epsilon_y^* - k_x k_z \epsilon_z \epsilon_y^* \right) \right. \\ \left. \times \left(\langle I | r^2 C_{2,1}^* G^+ r^2 C_{2,1} | I \rangle - \langle I | r^2 C_{2,-1}^* G^+ r^2 C_{2,-1} | I \rangle \right. \right. \\ \left. \left. + 2 \langle I | r^2 C_{2,2}^* G^+ r^2 C_{2,2} | I \rangle - 2 \langle I | r^2 C_{2,-2}^* G^+ r^2 C_{2,-2} | I \rangle \right) \right], \quad (4.60) \end{aligned}$$

$$\begin{aligned} \sigma(1, 1) = \pi^2 \alpha \hbar \omega k^2 \times \text{Im} \left[\frac{1}{40} \left((2k_x^2 + k_y^2 + 2k_z^2 - ik_x k_y) \epsilon_x^* \epsilon_z \right. \right. \\ \left. \left. - (2k_x^2 + k_y^2 + 2k_z^2 - ik_x k_y) \epsilon_x \epsilon_z^* - i(k_x^2 + 2k_y^2 + 2k_z^2 + ik_x k_y) \epsilon_y^* \epsilon_z \right. \right. \\ \left. \left. + i(k_x^2 + 2k_y^2 + 2k_z^2 + ik_x k_y) \epsilon_y \epsilon_z^* + (k_y + ik_x) k_z \epsilon_x^* \epsilon_y - i(k_x - ik_y) k_z \epsilon_x \epsilon_y^* \right) \right. \\ \left. \times \left(\sqrt{6} \langle I | r^2 C_{2,-1}^* G^+ r^2 C_{2,0} | I \rangle + \sqrt{6} \langle I | r^2 C_{2,0}^* G^+ r^2 C_{2,-1} | I \rangle \right. \right. \\ \left. \left. + 2 \langle I | r^2 C_{2,-2}^* G^+ r^2 C_{2,-1} | I \rangle + 2 \langle I | r^2 C_{2,1}^* G^+ r^2 C_{2,2} | I \rangle \right) \right], \quad (4.61) \end{aligned}$$

$$\begin{aligned} \sigma(1, -1) = \pi^2 \alpha \hbar \omega k^2 \times \text{Im} \left[\frac{-1}{40} \left((2k_x^2 + k_y^2 + 2k_z^2 + ik_x k_y) \epsilon_x^* \epsilon_z \right. \right. \\ \left. \left. - (2k_x^2 + k_y^2 + 2k_z^2 + ik_x k_y) \epsilon_x \epsilon_z^* + i(k_x^2 + 2k_y^2 + 2k_z^2 - ik_x k_y) \epsilon_y^* \epsilon_z \right. \right. \\ \left. \left. - i(k_x^2 + 2k_y^2 + 2k_z^2 - ik_x k_y) \epsilon_y \epsilon_z^* + k_z(k_y - ik_x) \epsilon_x^* \epsilon_y + ik_z(k_x + ik_y) \epsilon_x \epsilon_y^* \right) \right. \\ \left. \times \left(\sqrt{6} \langle I | r^2 C_{2,1}^* G^+ r_{2,0}^C | I \rangle + \sqrt{6} \langle I | r^2 C_{2,0}^* G^+ r^2 C_{2,-1} | I \rangle \right. \right. \\ \left. \left. + 2 \langle I | r^2 C_{2,2}^* G^+ r^2 C_{2,1} | I \rangle + 2 \langle I | r^2 C_{2,-1}^* G^+ r^2 C_{2,-2} | I \rangle \right) \right]. \quad (4.62) \end{aligned}$$

A quick check of (4.60), (4.61) and (4.62) reveals that the term $a = 1$ is zero for linear light. This implies that these fundamental spectra can only be probed with circular or elliptically polarized light. It is also clear that if the conductivity tensor has no off-diagonal terms, and satisfies

$$\begin{aligned} \langle I | r^2 C_{2,1}^* G^+ r^2 C_{2,1} | I \rangle &= \langle I | r^2 C_{2,-1}^* G^+ r^2 C_{2,-1} | I \rangle, \\ \langle I | r^2 C_{2,2}^* G^+ r^2 C_{2,2} | I \rangle &= \langle I | r^2 C_{2,-2}^* G^+ r^2 C_{2,-2} | I \rangle, \end{aligned}$$

then the term $a = 1$ is again zero.

4.2.5 Term $a = 2$

The term $a = 2$ consists of five components, namely, $\sigma(2, 0)$, $\sigma(2, 1)$, $\sigma(2, -1)$, $\sigma(2, 2)$, and $\sigma(2, -2)$

$$\begin{aligned}
 \sigma(2, 0) = & \pi^2 \alpha \hbar \omega k^2 \times \text{Im} \left[\frac{1}{84} \left((4k_x^2 \epsilon_x - 2k_x k_y \epsilon_y + k_x k_z \epsilon_z + 6k_y^2 \epsilon_x - 3k_z^2 \epsilon_x) \epsilon_x^* \right. \right. \\
 & + (6k_x^2 \epsilon_y - 2k_x k_y \epsilon_x + 4k_y^2 \epsilon_y + k_y k_z \epsilon_z - 3k_z^2 \epsilon_y) \epsilon_y^* \\
 & + (-3k_x^2 \epsilon_z + k_x k_z \epsilon_x - 3k_y^2 \epsilon_z + k_y k_z \epsilon_y - 8k_z^2 \epsilon_z) \epsilon_z^* \left. \right) \\
 & \times \left(2 \langle I | r^2 C_{2,2}^* G^+ r^2 C_{2,2} | I \rangle + 2 \langle I | r^2 C_{2,-2}^* G^+ r^2 C_{2,-2} | I \rangle \right. \\
 & - 2 \langle I | r^2 C_{2,0}^* G^+ r^2 C_{2,0} | I \rangle - \langle I | r^2 C_{2,1}^* G^+ r^2 C_{2,1} | I \rangle \\
 & \left. \left. - \langle I | r^2 C_{2,-1}^* G^+ r^2 C_{2,-1} | I \rangle \right) \right], \tag{4.63}
 \end{aligned}$$

$$\begin{aligned}
 \sigma(2, 1) = & \pi^2 \alpha \hbar \omega k^2 \times \text{Im} \left[\frac{-1}{168} \left([(4k_x \epsilon_x - 6ik_y \epsilon_x + ik_x \epsilon_y - ky \epsilon_y) k_z \right. \right. \\
 & + (2k_x^2 + ik_x k_y + 3k_y^2 + 2k_z^2) \epsilon_z] \epsilon_x^* - i [(-k_x \epsilon_x - ik_y \epsilon_x + 6ik_x \epsilon_y + 4ky \epsilon_y) k_z \\
 & + (3k_x^2 - ik_x k_y + 2(k_y^2 + k_z^2)) \epsilon_z] \epsilon_y^* + [2k_z^2 (\epsilon_x - i \epsilon_y) + k_y^2 (3\epsilon_x - 2i \epsilon_y) \\
 & + k_x^2 (2\epsilon_x - 3i \epsilon_y) - 4ik_y k_z \epsilon_z + k_x (ik_y \epsilon_x - ky \epsilon_y + 4k_z \epsilon_z)] \epsilon_z^* \left. \right) \\
 & \times \left(\sqrt{6} \langle I | r^2 C_{2,0}^* G^+ r^2 C_{2,1} | I \rangle - \sqrt{6} \langle I | r^2 C_{2,-1}^* G^+ r^2 C_{2,0} | I \rangle \right. \\
 & \left. \left. + 6 \langle I | r^2 C_{2,1}^* G^+ r^2 C_{2,2} | I \rangle - 6 \langle I | r^2 C_{2,-2}^* G^+ r^2 C_{2,-1} | I \rangle \right) \right], \tag{4.64}
 \end{aligned}$$

$$\begin{aligned}
 \sigma(2, -1) = & \pi^2 \alpha \hbar \omega k^2 \times \text{Im} \left[\frac{1}{168} \left([6ik_y k_z \epsilon_x - k_y k_z \epsilon_y + 2k_x^2 \epsilon_z + 3k_y^2 \epsilon_z + 2k_z^2 \epsilon_z \right. \right. \\
 & - ik_x (4ik_z \epsilon_x + k_z \epsilon_y + k_y \epsilon_z)] \epsilon_x^* + i [-k_x k_z (\epsilon_x + 6i \epsilon_y) + k_y k_z (i \epsilon_x + 4 \epsilon_y) \\
 & + 3k_x^2 \epsilon_z + ik_x k_y \epsilon_z + 2(k_y^2 + k_z^2) \epsilon_z] \epsilon_y^* + [2k_z^2 (\epsilon_x + i \epsilon_y) + k_y^2 (3\epsilon_x + 2i \epsilon_y) \\
 & + k_x^2 (2\epsilon_x + 3i \epsilon_y) + 4ik_y k_z \epsilon_z + k_x (-ik_y \epsilon_x - ky \epsilon_y + 4k_z \epsilon_z)] \epsilon_z^* \left. \right) \\
 & \times \left(\sqrt{6} \langle I | r^2 C_{2,0}^* G^+ r^2 C_{2,-1} | I \rangle - \sqrt{6} \langle I | r^2 C_{2,1}^* G^+ r^2 C_{2,0} | I \rangle \right. \\
 & \left. \left. + 6 \langle I | r^2 C_{2,-1}^* G^+ r^2 C_{2,-2} | I \rangle - 6 \langle I | r^2 C_{2,2}^* G^+ r^2 C_{2,1} | I \rangle \right) \right], \tag{4.65}
 \end{aligned}$$

$$\begin{aligned}
\sigma(2, 2) = & \pi^2 \alpha \hbar \omega k^2 \times \text{Im} \left[\frac{1}{4\sqrt{21}} \left(-2(k_x - ik_y)(\epsilon_x^* - i\epsilon_y^*)(k_x \epsilon_x + k_y \epsilon_y - 2k_z \epsilon_z) \right. \right. \\
& -3(\epsilon_z(k_x - ik_y) + k_z(\epsilon_x - i\epsilon_y))(\epsilon_z^*(k_x - ik_y) + k_z \epsilon_x^* - ik_z \epsilon_y^*) \\
& \left. \left. -2(k_x - ik_y)(\epsilon_x - i\epsilon_y)(k_x \epsilon_x^* + k_y \epsilon_y^* - 2k_z \epsilon_z^*) \right) \right. \\
& \times \left(\sqrt{\frac{2}{7}} \langle I | r^2 C_{2,0}^* G^+ r^2 C_{2,2} | I \rangle + \sqrt{\frac{3}{7}} \langle I | r^2 C_{2,-1}^* G^+ r^2 C_{2,1} | I \rangle \right. \\
& \left. \left. + \sqrt{\frac{2}{7}} \langle I | r^2 C_{2,-2}^* G^+ r^2 C_{2,0} | I \rangle \right) \right], \tag{4.66}
\end{aligned}$$

$$\begin{aligned}
\sigma(2, -2) = & \pi^2 \alpha \hbar \omega k^2 \times \text{Im} \left[\frac{1}{4\sqrt{21}} \left(-2(k_x + ik_y)(\epsilon_x^* + i\epsilon_y^*)(k_x \epsilon_x + k_y \epsilon_y - 2k_z \epsilon_z) \right. \right. \\
& -3(\epsilon_z(k_x + ik_y) + k_z(\epsilon_x + i\epsilon_y))(\epsilon_z^*(k_x + ik_y) + k_z \epsilon_x^* + ik_z \epsilon_y^*) \\
& \left. \left. -2(k_x + ik_y)(\epsilon_x + i\epsilon_y)(k_x \epsilon_x^* + k_y \epsilon_y^* - 2k_z \epsilon_z^*) \right) \right. \\
& \times \left(\sqrt{\frac{2}{7}} \langle I | r^2 C_{2,0}^* G^+ r^2 C_{2,-2} | I \rangle + \sqrt{\frac{3}{7}} \langle I | r^2 C_{2,1}^* G^+ r^2 C_{2,-1} | I \rangle \right. \\
& \left. \left. + \sqrt{\frac{2}{7}} \langle I | r^2 C_{2,2}^* G^+ r^2 C_{2,0} | I \rangle \right) \right]. \tag{4.67}
\end{aligned}$$

4.2.6 Term $a = 3$

The term $a = 3$ consists of seven components, namely, $\sigma(3, 0)$, $\sigma(3, 1)$, $\sigma(3, -1)$, $\sigma(3, 2)$, $\sigma(3, -2)$, $\sigma(3, 3)$, and $\sigma(3, -3)$

$$\begin{aligned}
\sigma(3, 0) = & \pi^2 \alpha \hbar \omega k^2 \times \text{Im} \left[\frac{i}{20} \left((k_x^2 + k_y^2 - 2k_z^2) \epsilon_x \epsilon_y^* - (k_x^2 + k_y^2 - 2k_z^2) \epsilon_y \epsilon_x^* \right. \right. \\
& \left. \left. + 2k_x k_z \epsilon_y \epsilon_z^* - 2k_x k_z \epsilon_z \epsilon_y^* + 2k_y k_z \epsilon_z \epsilon_x^* - 2k_y k_z \epsilon_x \epsilon_z^* \right) \right. \\
& \times \left(2 \langle I | r^2 C_{2,-1}^* G^+ r^2 C_{2,-1} | I \rangle - 2 \langle I | r^2 C_{2,1}^* G^+ r^2 C_{2,1} | I \rangle \right. \\
& \left. \left. + \langle I | r^2 C_{2,2}^* G^+ r^2 C_{2,2} | I \rangle - \langle I | r^2 C_{2,-2}^* G^+ r^2 C_{2,-2} | I \rangle \right) \right], \tag{4.68}
\end{aligned}$$

$$\begin{aligned}
\sigma(3, 1) = \pi^2 \alpha \hbar \omega k^2 \times \text{Im} & \left[\frac{1}{40\sqrt{6}} \left(i(3k_x^2 - 2ik_x k_y + k_y^2 - 4k_z^2) \epsilon_z \epsilon_y^* \right. \right. \\
& + 8k_z(k_y + ik_x) \epsilon_x \epsilon_y^* - (k_x^2 + 2ik_x k_y + 3k_y^2 - 4k_z^2) \epsilon_x^* \epsilon_z - 8k_z(k_y + ik_x) \epsilon_y \epsilon_x^* \\
& + \epsilon_z^* [k_x^2(\epsilon_x - 3i\epsilon_y) + 2ik_x k_y(\epsilon_x + i\epsilon_y) + k_y^2(3\epsilon_x - i\epsilon_y) - 4k_z^2(\epsilon_x - i\epsilon_y)] \\
& \times \left(2\langle I|r^2 C_{2,0}^* G^+ r^2 C_{2,1}|I \rangle + 2\langle I|r^2 C_{2,-1}^* G^+ r^2 C_{2,0}|I \rangle \right. \\
& \left. \left. - \sqrt{6}\langle I|r^2 C_{2,1}^* G^+ r^2 C_{2,2}|I \rangle - \sqrt{6}\langle I|r^2 C_{2,-2}^* G^+ r^2 C_{2,-1}|I \rangle \right) \right], \quad (4.69)
\end{aligned}$$

$$\begin{aligned}
\sigma(3, -1) = \pi^2 \alpha \hbar \omega k^2 \times \Im & \left[\frac{1}{40\sqrt{6}} \left(i(3k_x^2 + 2ik_x k_y + k_y^2 - 4k_z^2) \epsilon_y^* \epsilon_z \right. \right. \\
& + 8ik_z(k_x + ik_y) \epsilon_x \epsilon_y^* + (k_x^2 - 2ik_x k_y + 3k_y^2 - 4k_z^2) \epsilon_x^* \epsilon_z + 8k_z(k_y - ik_x) \epsilon_x^* \epsilon_y \\
& + \epsilon_z^* [k_x^2(-\epsilon_x + 3i\epsilon_y) + 2k_x k_y(\epsilon_y + i\epsilon_x) - k_y^2(3\epsilon_x + i\epsilon_y) + 4k_z^2(\epsilon_x + i\epsilon_y)] \\
& \times \left(2\langle I|r^2 C_{2,0}^* G^+ r^2 C_{2,-1}|I \rangle + 2\langle I|r^2 C_{2,1}^* G^+ r^2 C_{2,0}|I \rangle \right. \\
& \left. \left. - \sqrt{6}\langle I|r^2 C_{2,-1}^* G^+ r^2 C_{2,-2}|I \rangle - \sqrt{6}\langle I|r^2 C_{2,2}^* G^+ r^2 C_{2,1}|I \rangle \right) \right], \quad (4.70)
\end{aligned}$$

$$\begin{aligned}
\sigma(3, 2) = \pi^2 \alpha \hbar \omega k^2 \times \text{Im} & \left[\frac{1}{4\sqrt{6}} (k_y + ik_x) \left(\epsilon_x^*(k_x \epsilon_y - ik_y \epsilon_y + 2ik_z \epsilon_z) \right. \right. \\
& + \epsilon_y^*(-k_x \epsilon_x + ik_y \epsilon_x + 2k_z \epsilon_z) - 2ik_z \epsilon_z^*(\epsilon_x - i\epsilon_y) \\
& \left. \times \left(\langle I|r^2 C_{2,0}^* G^+ r^2 C_{2,2}|I \rangle - \langle I|r^2 C_{2,-2}^* G^+ r^2 C_{2,0}|I \rangle \right) \right], \quad (4.71)
\end{aligned}$$

$$\begin{aligned}
\sigma(3, -2) = \pi^2 \alpha \hbar \omega k^2 \times \text{Im} & \left[\frac{1}{4\sqrt{6}} (ik_y + k_x) \left(\epsilon_x^*(ik_x \epsilon_y - k_y \epsilon_y + 2k_z \epsilon_z) \right. \right. \\
& + \epsilon_y^*(-ik_x \epsilon_x + k_y \epsilon_x + 2ik_z \epsilon_z) - 2k_z \epsilon_z^*(\epsilon_x + i\epsilon_y) \\
& \left. \times \left(\langle I|r^2 C_{2,2}^* G^+ r^2 C_{2,0}|I \rangle - \langle I|r^2 C_{2,0}^* G^+ r^2 C_{2,-2}|I \rangle \right) \right], \quad (4.72)
\end{aligned}$$

$$\begin{aligned}
\sigma(3, 3) = \pi^2 \alpha \hbar \omega k^2 \times \text{Im} & \left[\frac{1}{8} \left((k_x - ik_y)^2 \right) \left(-\epsilon_z^*(\epsilon_x - i\epsilon_y) + \epsilon_z(\epsilon_x^* - i\epsilon_y^*) \right) \right. \\
& \left. \times \left(-\langle I|r^2 C_{2,-1}^* G^+ r^2 C_{2,2}|I \rangle - \langle I|r^2 C_{2,-2}^* G^+ r^2 C_{2,1}|I \rangle \right) \right], \quad (4.73)
\end{aligned}$$

$$\begin{aligned} \sigma(3, -3) = \pi^2 \alpha \hbar \omega k^2 \times \text{Im} \left[\frac{1}{8} \left((k_x + ik_y)^2 \right) \left(-\epsilon_z^* (\epsilon_x + i\epsilon_y) + \epsilon_z (\epsilon_x^* + i\epsilon_y^*) \right) \right. \\ \left. \times \left(\langle I | r^2 C_{2,1}^* G^+ r^2 C_{2,-2} | I \rangle + \langle I | r^2 C_{2,2}^* G^+ r^2 C_{2,-1} | I \rangle \right) \right]. \quad (4.74) \end{aligned}$$

4.2.7 Term $a = 4$

The term $a = 4$ consists of nine components, namely, $\sigma(4, 0)$, $\sigma(4, 1)$, $\sigma(4, -1)$, $\sigma(4, 2)$, $\sigma(4, -2)$, $\sigma(4, 3)$, $\sigma(4, -3)$, $\sigma(4, 4)$, and $\sigma(4, -4)$

$$\begin{aligned} \sigma(4, 0) = \pi^2 \alpha \hbar \omega k^2 \times \text{Im} \left[\frac{1}{140} \left([3k_x^2 \epsilon_x + k_y^2 \epsilon_x - 4k_z^2 \epsilon_x + 2k_x k_y \epsilon_y - 8k_x k_z \epsilon_z] \epsilon_x^* \right. \right. \\ \left. \left. + [k_x^2 \epsilon_y + 3k_y^2 \epsilon_y - 4k_z^2 \epsilon_y + 2k_x k_y \epsilon_x - 8k_y k_z \epsilon_z] \epsilon_y^* \right. \right. \\ \left. \left. - 4\epsilon_z^* [\epsilon_z (k_x^2 + k_y^2 - 2k_z^2) + 2k_z (k_x \epsilon_x + k_y \epsilon_y)] \right) \right. \\ \left. \times \left(6 \langle I | r^2 C_{2,0}^* G^+ r^2 C_{2,0} | I \rangle - 4 \langle I | r^2 C_{2,1}^* G^+ r^2 C_{2,1} | I \rangle \right. \right. \\ \left. \left. - 4 \langle I | r^2 C_{2,-1}^* G^+ r^2 C_{2,-1} | I \rangle + \langle I | r^2 C_{2,2}^* G^+ r^2 C_{2,2} | I \rangle \right. \right. \\ \left. \left. + \langle I | r^2 C_{2,-2}^* G^+ r^2 C_{2,-2} | I \rangle \right) \right], \quad (4.75) \end{aligned}$$

$$\begin{aligned} \sigma(4, 1) = \pi^2 \alpha \hbar \omega k^2 \times \text{Im} \left[\frac{1}{56} \left(\epsilon_x^* [3k_x^2 \epsilon_z - 2ik_x (k_y \epsilon_z + 3ik_z \epsilon_x + k_z \epsilon_y) + \epsilon_z (k_y^2 - 4k_z^2) \right. \right. \\ \left. \left. + 2k_y k_z (\epsilon_y - i\epsilon_x)] - i\epsilon_y^* [\epsilon_z (k_x^2 + 2ik_x k_y + 3k_y^2 - 4k_z^2) \right. \right. \\ \left. \left. + 2k_z (k_x \epsilon_x + ik_x \epsilon_y + ik_y \epsilon_x + 3k_y \epsilon_y)] + \epsilon_z^* [k_x^2 (3\epsilon_x - i\epsilon_y) \right. \right. \\ \left. \left. + 2k_x k_y (\epsilon_y - i\epsilon_x) - 8k_x k_z \epsilon_z + k_y^2 (\epsilon_x - 3i\epsilon_y) + 8ik_y k_z \epsilon_z - 4k_z^2 (\epsilon_x - i\epsilon_y)] \right) \right. \\ \left. \times \left(\sqrt{6} \langle I | r^2 C_{2,0}^* G^+ r^2 C_{2,1} | I \rangle - \sqrt{6} \langle I | r^2 C_{2,-1}^* G^+ r^2 C_{2,0} | I \rangle \right. \right. \\ \left. \left. \langle I | r^2 C_{2,-2}^* G^+ r^2 C_{2,-1} | I \rangle - \langle I | r^2 C_{2,1}^* G^+ r^2 C_{2,2} | I \rangle \right) \right], \quad (4.76) \end{aligned}$$

$$\begin{aligned}
\sigma(4, -1) = & \pi^2 \alpha \hbar \omega k^2 \times \text{Im} \left[\frac{-1}{56} \left(\epsilon_x^* [\epsilon_z (3k_x^2 + 2ik_x k_y + k_y^2 - 4k_z^2) \right. \right. \\
& + 2k_z (3k_x \epsilon_x + ik_x \epsilon_y + ik_y \epsilon_x + k_y \epsilon_y)] + \epsilon_y^* [i\epsilon_z (k_x^2 - 2ik_x k_y + 3k_y^2 - 4k_z^2) \\
& + 2k_z (ik_x \epsilon_x + k_x \epsilon_y + k_y \epsilon_x + 3ik_y \epsilon_y)] + \epsilon_z^* [k_x^2 (3\epsilon_x + i\epsilon_y) \\
& + 2k_x k_y (\epsilon_y + i\epsilon_x) - 8k_x k_z \epsilon_z + k_y^2 (\epsilon_x + 3i\epsilon_y) - 8ik_y k_z \epsilon_z - 4k_z^2 (\epsilon_x + i\epsilon_y)] \Big) \\
& \times \left(\sqrt{6} \langle I | r^2 C_{2,0}^* G^+ r^2 C_{2,-1} | I \rangle - \sqrt{6} \langle I | r^2 C_{2,1}^* G^+ r^2 C_{2,0} | I \rangle \right. \\
& \left. \langle I | r^2 C_{2,2}^* G^+ r^2 C_{2,1} | I \rangle - \langle I | r^2 C_{2,-1}^* G^+ r^2 C_{2,-2} | I \rangle \right) \Big], \quad (4.77)
\end{aligned}$$

$$\begin{aligned}
\sigma(4, 2) = & \pi^2 \alpha \hbar \omega k^2 \times \text{Im} \left[\frac{1}{56} \left(- (k_x - ik_y) (\epsilon_x^* - i\epsilon_y^*) (k_x \epsilon_x + k_y \epsilon_y - 2k_z \epsilon_z) \right. \right. \\
& + 2[\epsilon_z (k_x - ik_y) + k_z (\epsilon_x - i\epsilon_y)] [\epsilon_z^* (k_x - ik_y) + k_z \epsilon_x^* - ik_z \epsilon_y^*] \\
& - (k_x - ik_y) (\epsilon_x - i\epsilon_y) (k_x \epsilon_x^* + k_y \epsilon_y^* - 2k_z \epsilon_z^*) \Big) \\
& \times \left(\sqrt{6} \langle I | r^2 C_{2,0}^* G^+ r^2 C_{2,2} | I \rangle + \sqrt{6} \langle I | r^2 C_{2,-2}^* G^+ r^2 C_{2,0} | I \rangle \right. \\
& \left. - 4 \langle I | r^2 C_{2,-1}^* G^+ r^2 C_{2,1} | I \rangle \right) \Big], \quad (4.78)
\end{aligned}$$

$$\begin{aligned}
\sigma(4, -2) = & \pi^2 \alpha \hbar \omega k^2 \times \text{Im} \left[\frac{1}{56} \left(- (k_x + ik_y) (\epsilon_x^* + i\epsilon_y^*) (k_x \epsilon_x + k_y \epsilon_y - 2k_z \epsilon_z) \right. \right. \\
& + 2[\epsilon_z (k_x + ik_y) + k_z (\epsilon_x + i\epsilon_y)] [\epsilon_z^* (k_x + ik_y) + k_z \epsilon_x^* + ik_z \epsilon_y^*] \\
& - (k_x + ik_y) (\epsilon_x + i\epsilon_y) (k_x \epsilon_x^* + k_y \epsilon_y^* - 2k_z \epsilon_z^*) \Big) \\
& \times \left(\sqrt{6} \langle I | r^2 C_{2,0}^* G^+ r^2 C_{2,-2} | I \rangle + \sqrt{6} \langle I | r^2 C_{2,2}^* G^+ r^2 C_{2,0} | I \rangle \right. \\
& \left. - 4 \langle I | r^2 C_{2,1}^* G^+ r^2 C_{2,-1} | I \rangle \right) \Big], \quad (4.79)
\end{aligned}$$

$$\begin{aligned}
\sigma(4, 3) = & \pi^2 \alpha \hbar \omega k^2 \times \text{Im} \left[\frac{-1}{8} (k_x - ik_y) \left((\epsilon_x^* - i\epsilon_y^*) (\epsilon_z (k_x - ik_y) \right. \right. \\
& + 2k_z (\epsilon_x - i\epsilon_y)) + \epsilon_z^* (k_x - ik_y) (\epsilon_x - i\epsilon_y) \Big) \\
& \times \left(\langle I | r^2 C_{2,-2}^* G^+ r^2 C_{2,1} | I \rangle - \langle I | r^2 C_{2,-1}^* G^+ r^2 C_{2,2} | I \rangle \right) \Big], \quad (4.80)
\end{aligned}$$

$$\begin{aligned} \sigma(4, -3) = \pi^2 \alpha \hbar \omega k^2 \times \text{Im} \left[\frac{1}{8} (k_x + ik_y) \left((\epsilon_x^* + i\epsilon_y^*) (\epsilon_z (k_x + ik_y) \right. \right. \\ \left. \left. + 2k_z (\epsilon_x + i\epsilon_y)) + \epsilon_z^* (k_x + ik_y) (\epsilon_x + i\epsilon_y) \right) \right. \\ \left. \times \left(\langle I | r^2 C_{2,2}^* G^+ r^2 C_{2,-1} | I \rangle - \langle I | r^2 C_{2,1}^* G^+ r^2 C_{2,-2} | I \rangle \right) \right], \quad (4.81) \end{aligned}$$

$$\begin{aligned} \sigma(4, 4) = \pi^2 \alpha \hbar \omega k^2 \times \text{Im} \left[\frac{1}{4} (k_x - ik_y)^2 (\epsilon_x - i\epsilon_y) (\epsilon_x^* - i\epsilon_y^*) \right. \\ \left. \times \left(\langle I | r^2 C_{2,-2}^* G^+ r^2 C_{2,2} | I \rangle \right) \right], \quad (4.82) \end{aligned}$$

$$\begin{aligned} \sigma(4, -4) = \pi^2 \alpha \hbar \omega k^2 \times \text{Im} \left[\frac{1}{4} (k_x + ik_y)^2 (\epsilon_x + i\epsilon_y) (\epsilon_x^* + i\epsilon_y^*) \right. \\ \left. \times \left(\langle I | r^2 C_{2,2}^* G^+ r^2 C_{2,-2} | I \rangle \right) \right]. \quad (4.83) \end{aligned}$$

In the most general case, the quadrupole XAS signal can be described using 25 fundamental spectra as given in (4.59)–(4.83). Although the expression seems at first sight complicated, major simplifications and intuitive conclusions can be made when one considers the symmetry of the absorbing system. We shall illustrate this in the following section.

4.2.7.1 Case Study of a d^9 Ion

As an example, we will study again a d^9 ion in different local symmetries.

Spherical Symmetry

We shall start with an isolated d^9 ion (i.e., spherical symmetry). The conductivity tensor of such an ion is shown in Fig. 4.11. The tensor consists of 25 elements that form the 25 fundamental spectra through appropriate linear combinations. Only the five diagonal elements are non-zero in this case and are all equal. This means that the only possibly active fundamental spectra are of the type $\sigma(a, 0)$ with $a = 0, 1, 2, 3, 4$. However, because all the diagonal elements are equal, only the fundamental spectrum $\sigma(0, 0)$ is non-zero. This fundamental spectrum has no angular dependence, hence this system is isotropic. It is not a surprising result that for a spherical system, no angular dependence would be observed.

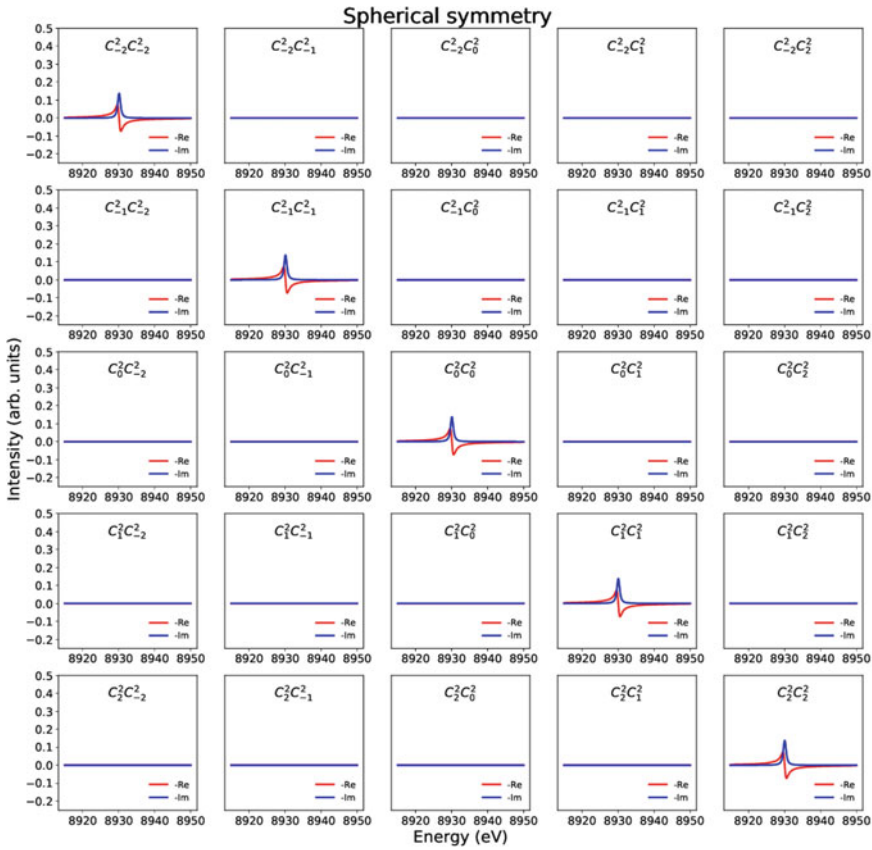


Fig. 4.11 Conductivity tensor calculated for a d^9 ion in spherical symmetry. Re and Im are the real and imaginary parts of the tensor

Octahedral Crystal Field

We shall examine next a d^9 ion in O_h symmetry. The conductivity tensor of this ion is shown in Fig. 4.12. Several differences can be directly seen in comparison with the previous case:

- The elements with the transition operator $T = C^2_{-2}$ are mixed with those of $T = C^2_2$.
- The diagonal elements are not equal.

Let us consider the first point. This mixing leads to the same form of eigenvectors than for obtained for the $3d$ orbitals ($Y_{2,m}$) for an O_h crystal field [see (4.23)]. Indeed, this is exactly the same problem. In order to obtain only diagonal elements, one can apply the following rotation (4.84):

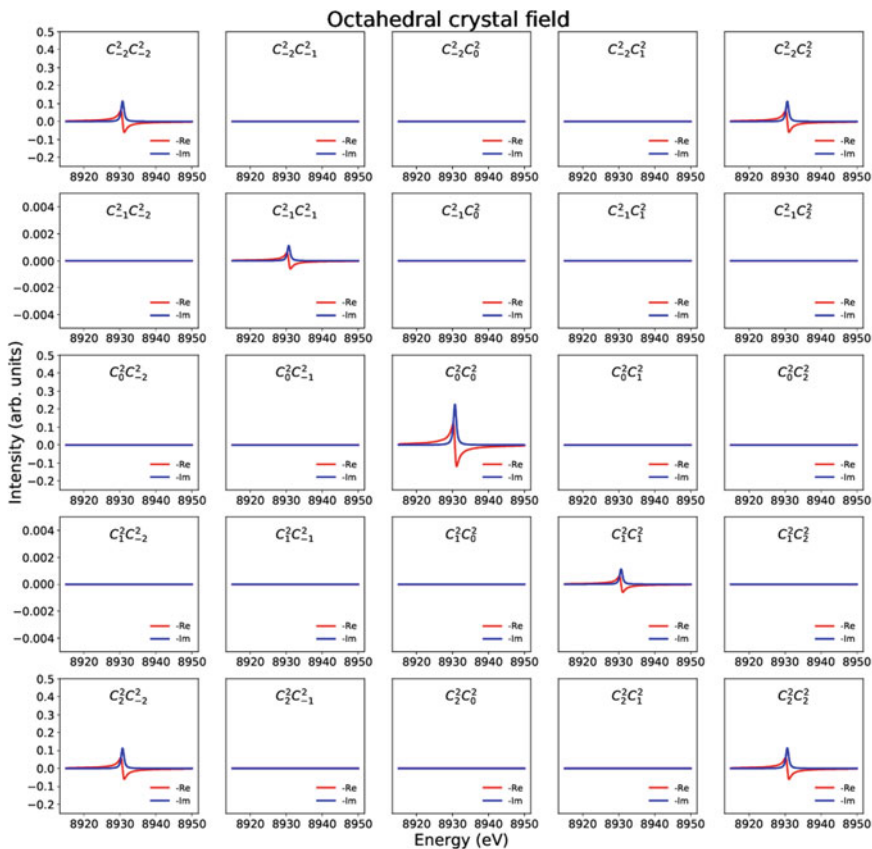


Fig. 4.12 Conductivity tensor of a d^9 ion in an octahedral crystal field ($10D_q = 1.1$ eV). Re and Im are the real and imaginary parts of the tensor

$$Rot = \begin{bmatrix} \frac{1}{\sqrt{2}} & 0 & 0 & 0 & \frac{1}{\sqrt{2}} \\ 0 & 0 & 1 & 0 & 0 \\ 0 & \frac{i}{\sqrt{2}} & 0 & \frac{i}{\sqrt{2}} & 0 \\ 0 & \frac{1}{\sqrt{2}} & 0 & -\frac{1}{\sqrt{2}} & 1 \\ \frac{i}{\sqrt{2}} & 0 & 0 & 0 & -\frac{i}{\sqrt{2}} \end{bmatrix}. \quad (4.84)$$

The rotated conductivity tensor is shown in Fig. 4.13. Only diagonal elements exist now. These are separated into two types: three (t_{2g}) that are equal with transition operators, C^2_{xy} , C^2_{yz} and C^2_{xz} , and two (e_g) that are equal with transition operators, $C^2_{z^2}$ and $C^2_{x^2-y^2}$.

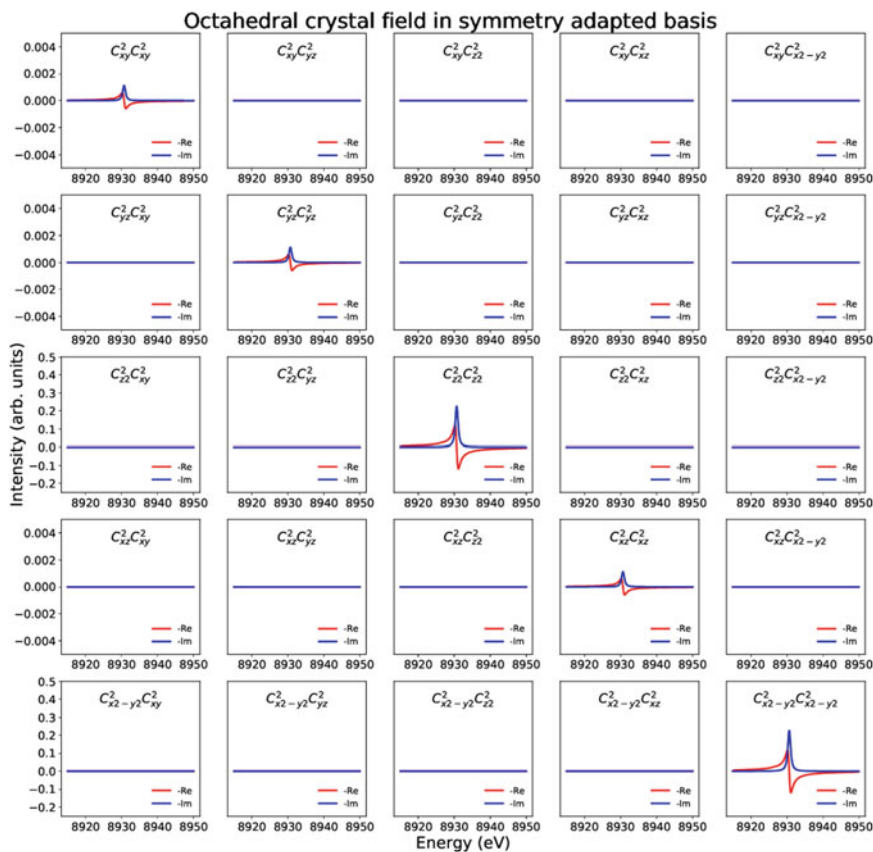


Fig. 4.13 Conductivity tensor for a d^9 ion in an octahedral crystal field ($10D_q = 1.1$ eV) calculated using the symmetry adapted basis set

Five fundamental spectra come into play, namely, $\sigma(0, 0)$, $\sigma(2, 0)$, $\sigma(4, 0)$, $\sigma(4, 4)$, and $\sigma(4, -4)$ as shown in Fig. 4.14. The O_h symmetry implies that $R(2, 0)$ is always equal to zero as confirmed by the calculation. In addition, $R(4, 4) = R(4, -4)$ and are proportional to $R(4, 0)$ as can be seen from (4.75), (4.82), and (4.83). Therefore, as can be expected from group theory, only two fundamental spectra are required to fully describe the system.

Let us investigate the angular dependence of a quadrupole transition in an O_h crystal field considering two scattering geometries. In the first geometry, the wave vector (\mathbf{k}) is aligned parallel to the [100] direction and the polarization (ϵ) is rotated in the $z - y$ -plane as illustrated in the right panel of Fig. 4.16. Despite the presence of non-isotropic fundamental spectra [$\sigma(4, 0)$, $\sigma(4, 4)$, and $\sigma(4, -4)$], the XAS cross-section is constant in these settings as shown in Fig. 4.16a. In the second geometry we

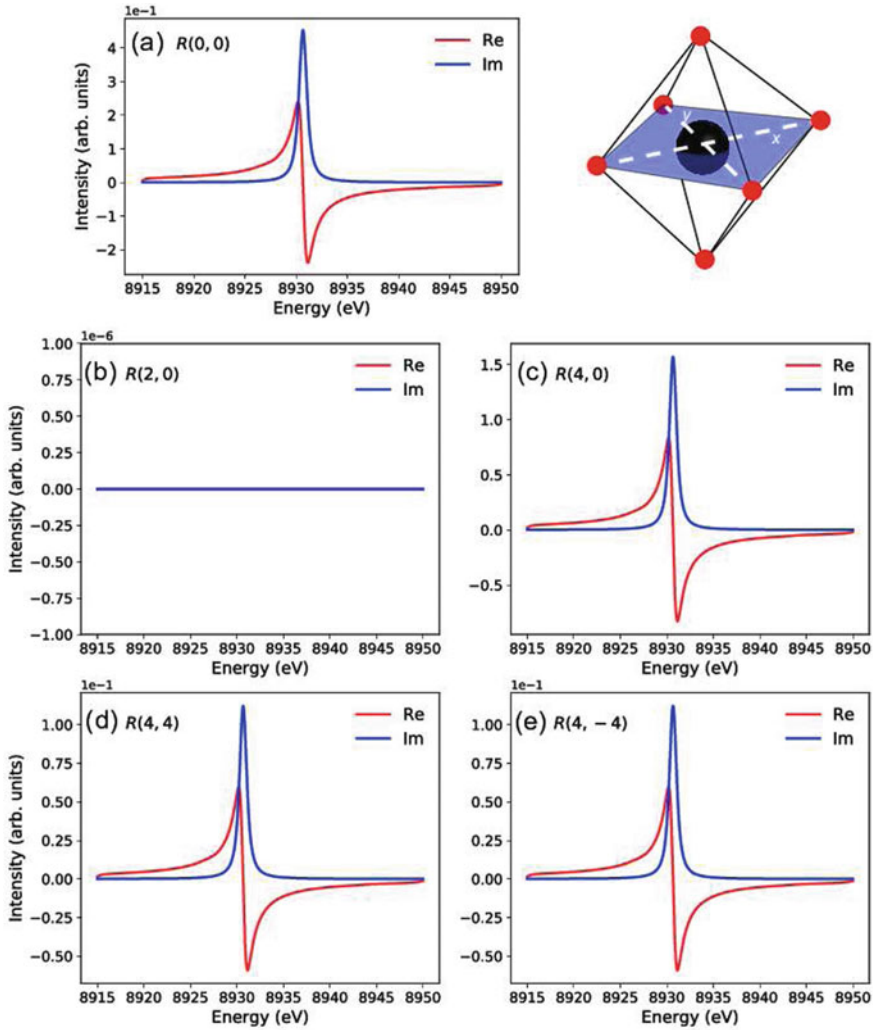


Fig. 4.14 Fundamental spectra for a quadrupole transition in a $3d^9$ ion in an octahedral crystal field. Re and Im are the real and imaginary parts of the spectra

have $\mathbf{k} \parallel [\frac{1}{\sqrt{2}} \frac{1}{\sqrt{2}} 0]$ and ϵ is rotated about the $[\frac{1}{\sqrt{2}} \frac{1}{\sqrt{2}} 0]$ axis as depicted in Fig. 4.16b. The XAS cross section shows a clear twofold angular dependence in these settings.

It is interesting to discuss the difference between both scattering geometries and the reason behind the absence of angular dependence in the first case. In Fig. 4.15, we plot the angular dependence of the light tensor [$E(4, 0)$, $E(4, 4)$, and $E(4, -4)$] for both cases. The contribution of the term $E(4, 0)$ is 90° out-of-phase with respect to the terms $E(4, 4)$ and $E(4, -4)$ for the first scattering geometry [see panel (a) of Fig. 4.15]. The O_h symmetry implies that the ratio between the $R(4, 0)$ and the

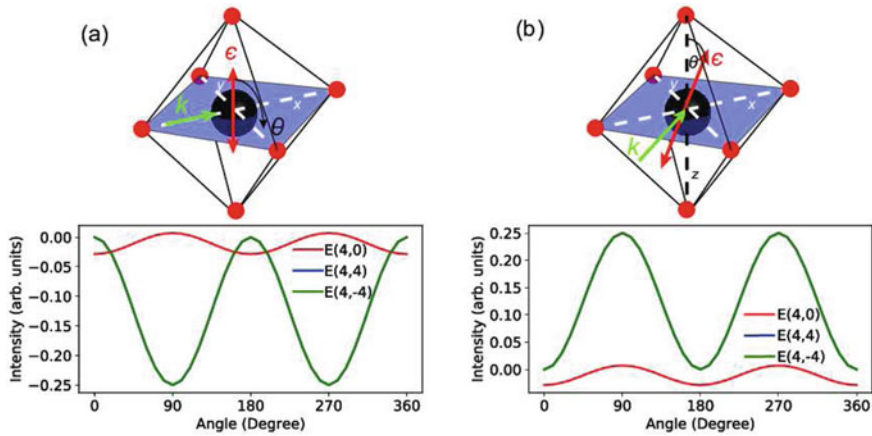


Fig. 4.15 Angular dependence of $E(4, 0)$, $E(4, 4)$, and $E(4, -4)$ terms. **a** The wave vector (k) is aligned with [100]. The angular dependence is computed by rotating the polarization (ϵ) about [100] with $\theta = 0^\circ$ for $\epsilon \parallel [001]$. **b** k is aligned with $[\frac{1}{\sqrt{2}} \frac{1}{\sqrt{2}} 0]$. The angular dependence is computed by rotating ϵ about $[\frac{1}{\sqrt{2}} \frac{1}{\sqrt{2}} 0]$ with $\theta = 0^\circ$ for $\epsilon \parallel [001]$

$R(4, \pm 4)$ terms leads to a constant XAS cross section. On the other hand, as depicted in Fig. 4.15b, all terms are in phase which leads to an angular dependent XAS.

An important distinction between the dipole and quadrupole transitions can be concluded from these examples. While a dipole transition in an O_h system exhibits no angular dependence, the quadrupole transition can show angular dependences when the scattering geometry is appropriately chosen. This difference holds because a quadrupole transition has higher multipole contributions that give rise to angular dependences not observable for dipole transitions.

Tetragonal Crystal Field

The effect of reducing the crystal field symmetry to tetragonal by applying a compressive distortion along the z -axis can be directly seen in the angular dependence of the quadrupole transition. In contrast to the case of O_h crystal field (see Fig. 4.16a), now rotating ϵ about the [100] axis shows angular dependence because the z - and y -axes are not equivalent (see Fig. 4.17a). However, as could be expected, rotating ϵ about the [001] axis shows no angular dependence (see Fig. 4.17b). In this projection, the system is effective of O_h symmetry.

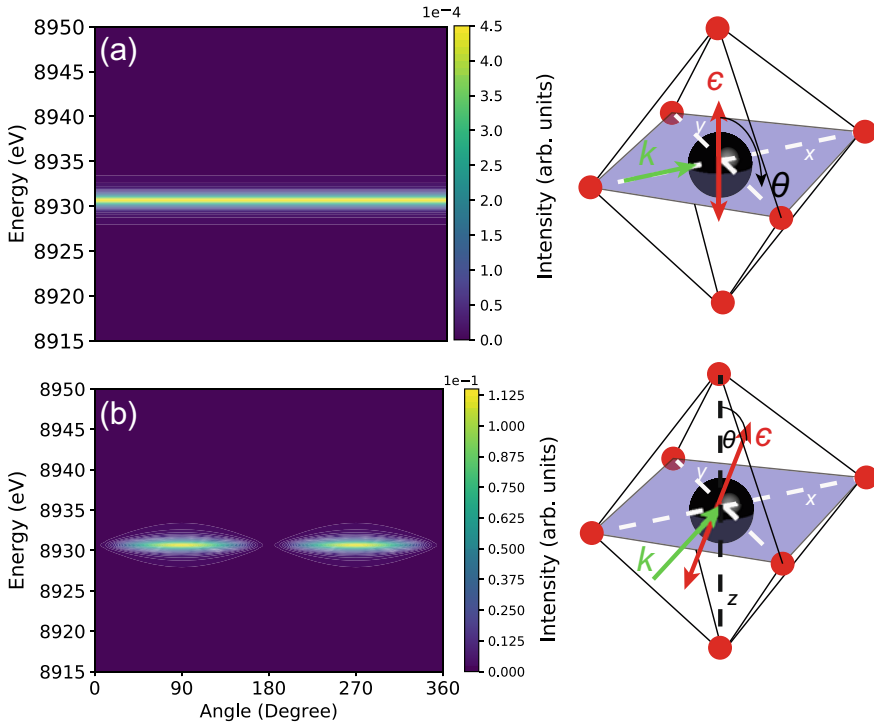


Fig. 4.16 Angular dependence of XAS for a quadrupole transition in a $3d^9 O_h$ ion with $10D_q = 1.1$ eV. **a** The wave vector (\mathbf{k}) is aligned with [100]. The angular dependence is computed by rotating the polarization vector (ϵ) about [100] with $\theta = 0^\circ$ for $\epsilon \parallel [001]$ as depicted in the sketch on the right. **b** \mathbf{k} is aligned with $[\frac{1}{\sqrt{2}} \frac{1}{\sqrt{2}} 0]$. The angular dependence is computed by rotating ϵ about $[\frac{1}{\sqrt{2}} \frac{1}{\sqrt{2}} 0]$ with $\theta = 0^\circ$ for $\epsilon \parallel [001]$ as depicted in the sketch on the right

Octahedral Crystal Field with Exchange Field $\parallel z$

Consider a magnetic $3d^9$ ion where the crystal field is O_h with an exchange field aligned along the z -axis. Seven fundamental spectra come into play, namely, $R(0, 0)$, $R(1, 0)$, $R(2, 0)$, $R(3, 0)$, $R(4, 0)$, $R(4, -4)$, and $R(4, 4)$. We have shown previously that for O_h symmetry, when \mathbf{k} is aligned parallel to the [100] direction, and ϵ is rotated in the $z - y$ -plane, angular dependence is observed (see Fig. 4.16a). Repeating the same calculation with an exchange field aligned along the z -axis leads to an angular dependent XAS as shown in Fig. 4.18a. The exchange field reduces the symmetry along the z -axis. The effects of rotating the incident linear polarization in the $z - y$ -plane on the fundamental cross sections are shown in Fig. 4.19. Only the terms $\sigma(2, 0)$, $\sigma(4, 0)$, $\sigma(4, 4)$, and $\sigma(4, -4)$ are non-zero and exhibit a twofold angular

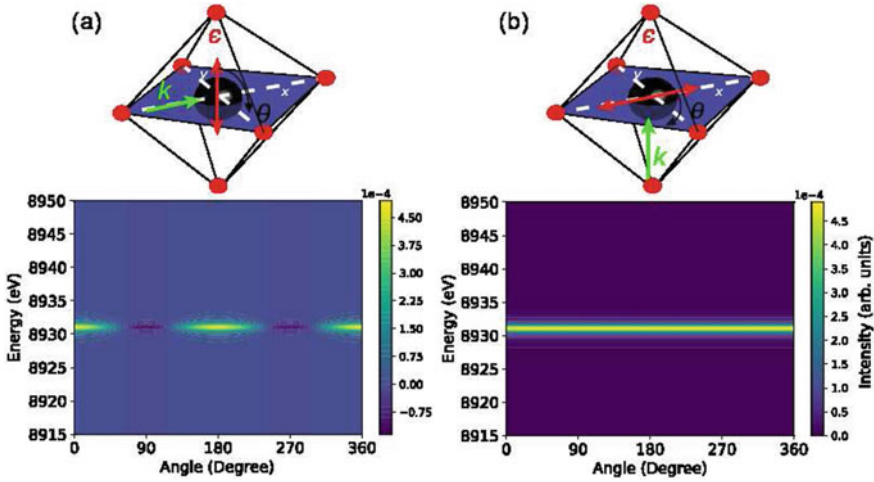


Fig. 4.17 Angular dependence of XAS for a quadrupole transition in a $3d^9$ ion in a D_{4h} crystal field ($10D_q = 1.1$ eV and $D_s = -0.2$ eV). **a** The wave vector (k) is aligned with $[100]$. The angular dependence is computed by rotating the polarization (ϵ) about $[100]$ with $\theta = 0^\circ$ for $\epsilon \parallel [001]$. **b** k is aligned with $[001]$ and ϵ is rotated about the $[001]$ with $\theta = 0^\circ$ for $\epsilon \parallel [100]$

dependence. However, one notes that $\sigma(4, 0)$ is 90° shifted with respect to $\sigma(4, 4)$ and $\sigma(4, -4)$ which implies that the angular dependence of the XAS will be small. In comparison, no angular dependence is observed when ϵ is rotated in the $x - y$ -plane as shown in Fig. 4.18b.

Finally, the exchange field can give rise to interesting combinations of structural and magnetic dichroism effects. Consider aligning $k \parallel [001]$ and measuring XAS using circular polarized light. Rotating the system about the $[100]$ axis gives rise to unconventional angular dependent XAS as shown in Fig. 4.20. This angular dependence arises from a combination of structural and magnetic dichroism effects.

The magnetic contribution arises from the circular dichroism active terms which are $\sigma(1, 0)$ and $\sigma(3, 0)$ (see Fig. 4.21a). On the other hand, the structural contribution arises from the linear dichroism active terms which are $\sigma(4, 0)$, $\sigma(4, 4)$, and $\sigma(4, -4)$ (see Fig. 4.21b). In addition, these terms contribute weakly to the magnetic dichroism.

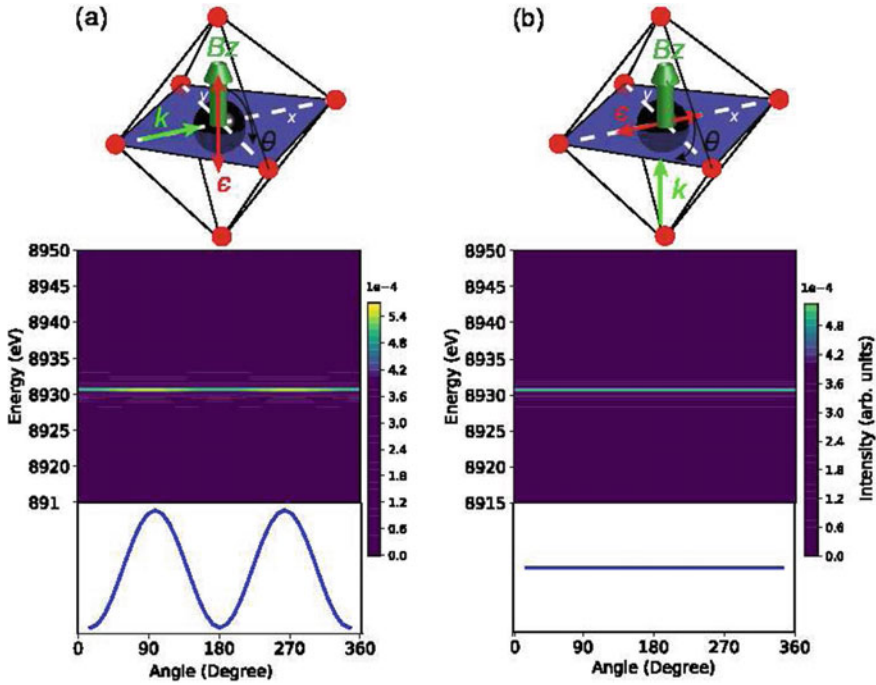


Fig. 4.18 Angular dependence of a quadrupole transition for a $3d^9$ ion in O_h crystal field ($10D_q = 1.1$ eV) with an exchange field aligned along the z -axis ($B = 0.05$ eV). **a** The wave vector (k) is aligned with [100]. The angular dependence is computed by rotating the polarization vector (ϵ) about [100] with $\theta = 0^\circ$ for $\epsilon \parallel [001]$. **b** k is aligned with [001] and ϵ is rotated about the [001] with $\theta = 0^\circ$ for $\epsilon \parallel [100]$

This is illustrated in Fig. 4.22 where in panel (a) we show the structural dichroism signal for the same system without an exchange field and in panel (b) the difference between the case with exchange versus without exchange. The magnetic contribution is about three orders of magnitude less than the structural contribution for this system.

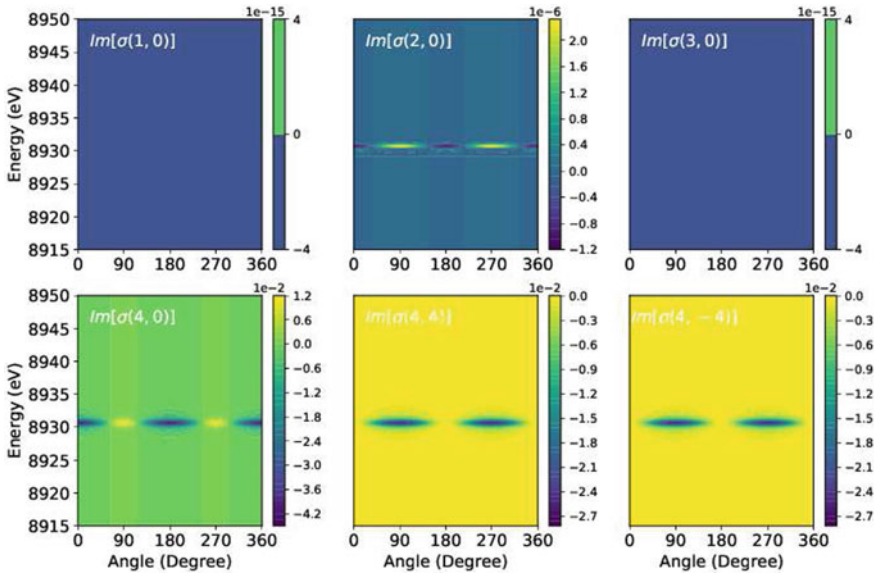


Fig. 4.19 Angular dependence of XAS fundamental cross sections $\sigma(1, 0)$, $\sigma(2, 0)$, $\sigma(3, 0)$, $\sigma(4, 0)$, $\sigma(4, 4)$, and $\sigma(4, -4)$. Here k is aligned with $[100]$ and ϵ is rotated about $[100]$ with $\theta = 0^\circ$ for $\epsilon \parallel [001]$

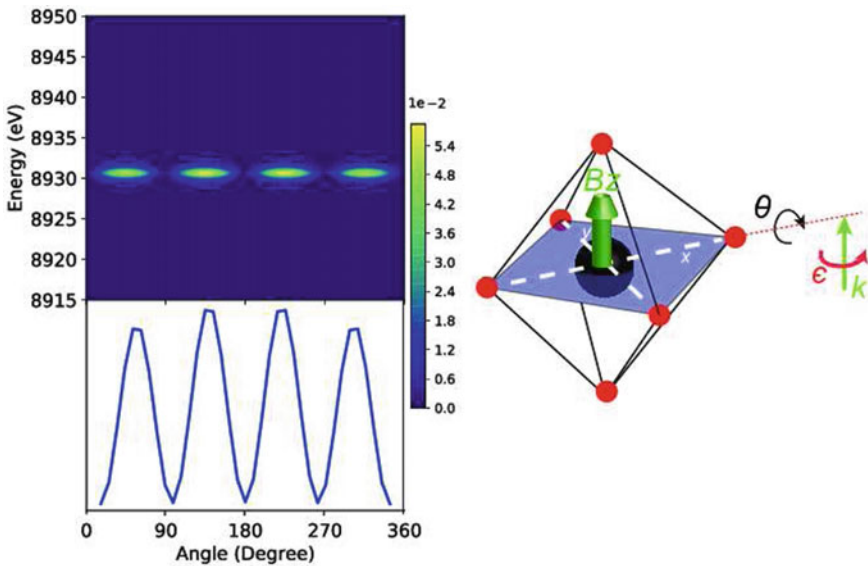


Fig. 4.20 Angular dependence of XAS for a quadrupole transition in a $3d^9$ ion in an O_h crystal field ($10D_q = 1.1$ eV) with an exchange field aligned along the z -axis ($B = 0.05$ eV). The wave vector (k) is initially aligned to $[001]$ and polarization (ϵ) is circular. The angular dependence is computed by rotating the system about the $[100]$ axis

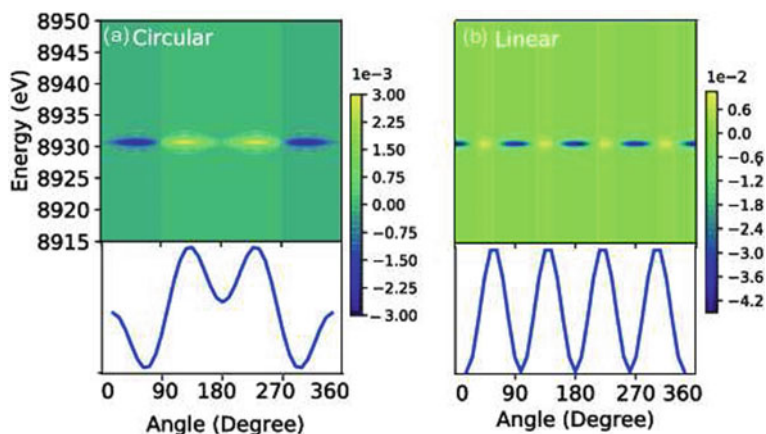


Fig. 4.21 Angular dependence of XAS fundamental spectra for a quadrupole transition in a $3d^9$ ion in an O_h crystal field with an exchange field aligned along the z -axis. **a** Circular dichroism active terms $\sigma(1, 0)$ and $\sigma(3, 0)$. **b** Linear dichroism active terms $\sigma(4, 0)$, $\sigma(4, 4)$ and $\sigma(4, -4)$. The angular dependence is computed by rotating the system about the $[100]$ axis

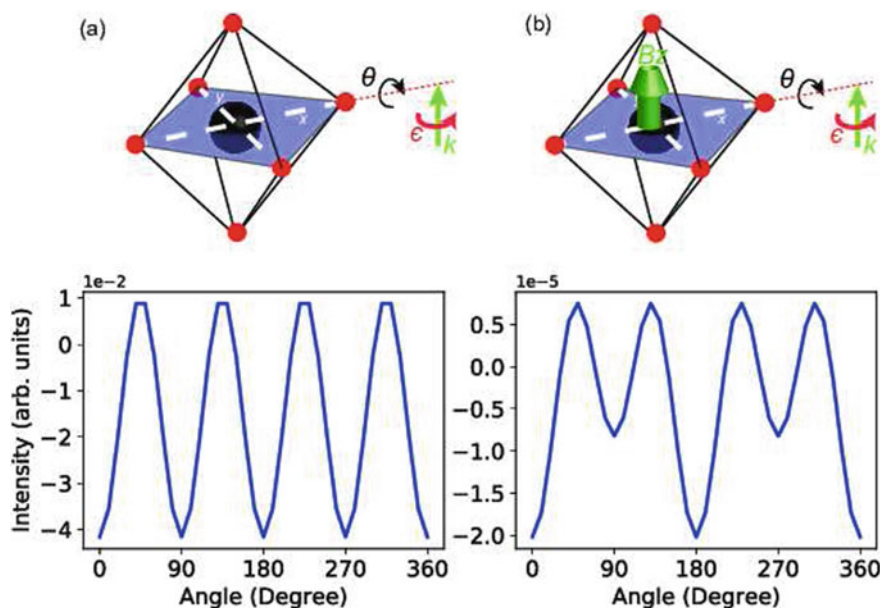


Fig. 4.22 Angular dependence of XAS for a quadrupole transition in a $3d^9$ ion: **a** in an O_h crystal field ($10D_q = 1.1$ eV). **b** The difference between calculation (a) and in an O_h crystal field with an exchange field aligned along the z -axis ($10D_q = 1.1$ eV and $B = 0.05$ eV). The wave vector (\mathbf{k}) is initially aligned to $[001]$ and polarization ($\boldsymbol{\epsilon}$) is circularly polarized. The angular dependence is computed by rotating the system about the $[100]$ axis

4.3 Conclusion

We have expressed the XAS cross section using Green's function formalism and spherical tensors, which allows a tractable investigation of the different types of dichroism: on the one hand experimentally, by allowing the experimentalist to predict the smallest set of measurements required to recover the full spectroscopic information and therefore to optimize beamtime; on the other hand theoretically, using modern core level spectroscopy codes, by allowing a more efficient calculation rather than a point-by-point time-consuming treatment. In a forthcoming work, we intend to use a similar approach for resonant inelastic X-ray scattering (RIXS) spectroscopy, whose richness lies in the large number of possible spectra that can be obtained by varying the energy, direction, and polarization state of the incident and scattered beams [28]. But as a matter of fact, there is so much information in the spectra that it is difficult to know whether a specific set of experiments measures all potential information. In our opinion, the possibilities offered by angular and polarization dependent RIXS measurements have not yet been exploited to the best of their potential. Nevertheless, the technique has now become mature and popular and will benefit from the huge instrumentation progress achieved in the last years, which open new doors for the exploration of dichroisms in materials.

References

1. C. Brouder, Angular dependence of X-ray absorption spectra. *J. Phys.: Condens. Matter* **2**, 701 (1990). <https://doi.org/10.1088/0953-8984/2/3/018>
2. A. Juhin, S.P. Collins, Y. Joly, M. Diaz-Lopez, K. Kvashnina, P. Glatzel, C. Brouder, F.M.F. de Groot, Measurement of f orbital hybridization in rare earths through electric dipole-octupole interference in X-ray absorption spectroscopy. *Phys. Rev. Mater.* **3**, 120801(R) (2019). <https://doi.org/10.1103/PhysRevMaterials.3.120801>
3. S. Sugano, T. Tanabe, H. Kamimura, *Multiplets of Transition Metal Ions in Crystals* (Academic, New York, 1970)
4. J.S. Griffith, *The Theory of Transition-Metal Ions* (Cambridge University Press, Cambridge, 1961)
5. E. König, S. Kremer, *Ligand Field Energy Diagrams* (Springer Science+Business Media, New York, 2013). <https://doi.org/10.1007/978-1-4757-1529-3>
6. R.D. Cowan, *The Theory of Atomic Structure and Spectra* (University of California Press, Berkeley, 1981)
7. M.W. Haverkort, Y. Lu, S. Macke, R. Green, M. Brass, S. Heinze, Quany – a quantum many body script language, <http://www.quany.org/doku.php?id=start&rev=1522759229>
8. M. Baer, Multipole expansion package, <https://github.com/maroba/multipoles>
9. M.W. Haverkort, M. Zwierzycki, O.K. Andersen, Multiplet ligand-field theory using Wannier orbitals. *Phys. Rev. B* **85**, 165113 (2012). <https://doi.org/10.1103/PhysRevB.85.165113>
10. Y. Lu, M. Höppner, O. Gunnarsson, M.W. Haverkort, Efficient real-frequency solver for dynamical mean-field theory. *Phys. Rev. B* **90**, 085102 (2014). <https://doi.org/10.1103/PhysRevB.90.085102>
11. M.W. Haverkort, G. Sangiovanni, P. Hansmann, A. Toschi, Y. Lu, S. Macke, Bands, resonances, edge singularities and excitons in core level spectroscopy investigated within the dynamical

- mean-field theory. *Europhys. Lett.* **108**, 57004 (2014). <https://doi.org/10.1209/0295-5075/108/57004>
12. M.W. Haverkort, Quanta for core level spectroscopy - excitons, resonances and band excitations in time and frequency domain. *J. Phys. Conf. Ser.* **712**, 012001 (2016). <https://doi.org/10.1088/1742-6596/712/1/012001>
 13. M. Retegan, Crispy: v0.7.3. <https://doi.org/10.5281/zenodo.1008184>
 14. C. Brouder, A. Juhin, A. Bordage, M.-A. Arrio, Site symmetry and crystal symmetry: a spherical tensor analysis. *J. Phys.: Condens. Matter* **20**, 455205 (2008). <https://doi.org/10.1088/0953-8984/20/45/455205>
 15. B.T. Thole, G. van der Laan, Spin polarization and magnetic dichroism in photoemission from core and valence states in localized magnetic systems. *Phys. Rev. B* **44**, 12424 (1991). <https://doi.org/10.1103/PhysRevB.44.12424>
 16. G. van der Laan, B.T. Thole, Spin polarization and magnetic dichroism in photoemission from core and valence states in localized magnetic systems. II. Emission from open shells. *Phys. Rev. B* **48**, 210 (1993). <https://doi.org/10.1103/PhysRevB.48.210>
 17. B.T. Thole, G. van der Laan, Spin polarization and magnetic dichroism in photoemission from core and valence states in localized magnetic systems. III. Angular distributions. *Phys. Rev. B* **49**, 9613 (1994). <https://doi.org/10.1103/PhysRevB.49.9613>
 18. G. van der Laan, B.T. Thole, Spin polarization and magnetic dichroism in photoemission from core and valence states in localized magnetic systems. IV. Core-hole polarization in resonant photoemission. *Phys. Rev. B* **52**, 15355 (1995). <https://doi.org/10.1103/PhysRevB.52.15355>
 19. G. van der Laan, B.T. Thole, Core hole polarization in resonant photoemission. *J. Phys. Condens. Matter* **7**, 9947 (1995). <https://doi.org/10.1088/0953-8984/7/50/028>
 20. P. Carra, H. König, B.T. Thole, M. Altarelli, Magnetic X-ray dichroism: general features of dipolar and quadrupolar spectra. *Physica B* **192**, 182 (1993). [https://doi.org/10.1016/0921-4526\(93\)90119-Q](https://doi.org/10.1016/0921-4526(93)90119-Q)
 21. J.-P. Schill e J.-P. Kappler, P. Sainctavit, C. Cartier dit Moulin, C. Brouder, G. Krill, Experimental and calculated magnetic dichroism in the Ho 3d X-ray absorption of intermetallic HoCo₂. *Phys. Rev. B* **48**, 9491 (1993). <https://doi.org/10.1103/PhysRevB.48.9491>
 22. B.T. Thole, G. van der Laan, M. Fabrizio, Magnetic ground-state properties and spectral distributions. I. X-ray-absorption spectra. *Phys. Rev. B* **50**, 11466 (1994). <https://doi.org/10.1103/PhysRevB.50.11466>
 23. A. Juhin, C. Brouder, M.-A. Arrio, D. Cabaret, P. Sainctavit, E. Balan, A. Bordage, A.P. Seitsonen, G. Calas, S.G. Eeckhout, P. Glatzel, X-ray linear dichroism in cubic compounds: the case of Cr³⁺ in MgAl₂O₄. *Phys. Rev. B* **78**, 195103 (2008). <https://doi.org/10.1103/PhysRevB.78.195103>
 24. G. van der Laan, Magnetic linear X-ray dichroism as a probe of the magnetocrystalline anisotropy. *Phys. Rev. Lett.* **82**, 640 (1999). <https://doi.org/10.1103/PhysRevLett.82.640>
 25. E. Arenholz, G. van der Laan, R.V. Chopdekar, Y. Suzuki, Anisotropic X-ray magnetic linear dichroism at the Fe L_{2,3} edges in Fe₃O₄. *Phys. Rev. B* **74**, 094407 (2006). <https://doi.org/10.1103/PhysRevB.74.094407>
 26. G. Sch utz, W. Wagner, W. Wilhelm, P. Kienle, R. Zeller, R. Frahm, G. Materlik, Absorption of circularly polarized X rays in iron. *Phys. Rev. Lett.* **58**, 737 (1987). <https://doi.org/10.1103/PhysRevLett.58.737>
 27. P. Carra, B.T. Thole, M. Altarelli, X. Wang, X-ray circular dichroism and local magnetic fields. *Phys. Rev. Lett.* **70**, 694 (1993). <https://doi.org/10.1103/PhysRevLett.70.694>
 28. A. Juhin, C. Brouder, F. de Groot, Angular dependence of resonant inelastic X-ray scattering: a spherical tensor expansion. *Cent. Eur. J. Phys.* **12**, 323 (2014). <https://doi.org/10.2478/s11534-014-0450-2>

Open Access This chapter is licensed under the terms of the Creative Commons Attribution 4.0 International License (<http://creativecommons.org/licenses/by/4.0/>), which permits use, sharing, adaptation, distribution and reproduction in any medium or format, as long as you give appropriate credit to the original author(s) and the source, provide a link to the Creative Commons license and indicate if changes were made.

The images or other third party material in this chapter are included in the chapter's Creative Commons license, unless indicated otherwise in a credit line to the material. If material is not included in the chapter's Creative Commons license and your intended use is not permitted by statutory regulation or exceeds the permitted use, you will need to obtain permission directly from the copyright holder.

